Author's response

Dear Editor,

Thanks for the detailed comments. We have now completed the technical corrections for our manuscript. In addition, we have also technically updated Fig. A1 by making the three composite panels into one file.

On behalf of the authors,
Yongbiao Weng
12 May 2020

Point-by-point response to editor's the comments

Received and published: 11 May 2020

P3 l30: please insert parentheses between equal (=) and times (x) sign for both ratios, 2R and 18R.

AUTHOR'S REPLY:
Done.

P4 l20: please use parantheses around value and uncertainty. Since the pressure unit is non-SI, please give the SI value in parentheses for the Torr reading.

AUTHOR'S REPLY:
Have added SI value. Also used parentheses for all the value and uncertainty expressions in the manuscript.

P6 l23: convert to pressure unit within SI (eg 170 hPa).

AUTHOR'S REPLY:
Done.

Fig. 5. y axis label : In accordance with the IUPAC gold book, define absorbance as ln(Io/I) and put the term in parentheses instead of separating by backslash, as the definition of a quantity does not constitute a unit.

AUTHOR'S REPLY:
Done.

Tables 2, 4 and 5: Please report significant figures according to SI and IUPAC recommendations (https://publications.copernicus.org/for_a
While the links on that page may not be specific enough, a more exhaustive source for the reporting of measurement results is the "Guide to the Expression of Uncertainty in Measurement" (https://www.bipm.org/en/publications/guides/gum.html) from which the following paragraph is taken.

7.2.6 The numerical values of the estimate y and its standard uncertainty uc(y) or expanded uncertainty U should not be given with an excessive number of digits. It usually suffices to quote uc(y) and U [as well as the standard uncertainties u(xi) of the input estimates xi] to at most two significant digits, although in some cases it may be necessary to retain additional digits to avoid round-off errors in subsequent calculations. In reporting final results, it may sometimes be appropriate to round uncertainties up rather than to the nearest digit. For example, uc(y) = 10,47 mΩ might be rounded up to 11 mΩ. However, common sense should prevail and a value such as u(xi) = 28,05 kHz should be rounded down to 28 kHz. Output and input estimates should be rounded to be consistent with their uncertainties; for example, if y = 10,057 62 Ω with uc(y) = 27 mΩ, y

should be rounded to 10,058 Ω. Correlation coefficients should be given with three-digit accuracy if their absolute values are near unity.

In Table 2, FARLAB standards are reported accordingly (with uncertainties and values given with the same number of signifcant digits and at most 1 redundant figure). However, deuterium compositions for UI standards are not (with uncertainty having one digit after the decimal point (0.6) as compared to values that have two).

In Tables 4 and 5, you should give -274.95 ± 16.62 as -295 ± 17, -2.60 10^5 ± 6.23 x 10^7 as 2.60 x 10^5 ± 7 x 10^7, 9511.99 ± 163.45 as 9510 ± 170 etc.

AUTHOR'S REPLY:

Only one digit after the decimal point has been originally reported for the uncertainty of δD of DI standards in Table 2. We therefore decided to now also report the δD of UI standards with one digit after the decimal point. We have changed the significant figures in Table 4 and 5 following the guidelines when applicable, i.e., keeping three significant figures, rounding up the uncertainty and keeping the consistency between the report value and its uncertainty.

Correcting the impact of the isotope composition on the mixing ratio dependency of water vapour isotope measurements with cavity ring–down spectrometers

Yongbiao Weng[1,2], Alexandra Touzeau[1,2], and Harald Sodemann[1,2]

[1]Geophysical Institute, University of Bergen, Bergen, Norway
[2]Bjerknes Centre for Climate Research, Bergen, Norway

Correspondence to: Yongbiao Weng (yongbiao.weng@uib.no)

Abstract.

Recent advances in laser spectroscopy enable high frequency in situ measurements of the isotope composition of water vapour. At low water vapour mixing ratios, however, the measured stable water isotope composition can be substantially affected by a measurement artefact known as the mixing ratio dependency, which is commonly considered independent of the isotope composition. Here we systematically investigate how the mixing ratio dependency in a range from 500 to $23'000$ ppmv of three commercial cavity ring–down spectrometers is affected by the isotope composition of water vapour. We find that the isotope composition of water vapour has a substantial and systematic impact on the mixing ratio dependency for all three analysers, in particular at mixing ratios below $4'000$ ppmv. This isotope composition dependency can create a deviation of ± 0.5 and ± 6.0 ‰ for δ^{18}O and δD respectively at $\sim 2'000$ ppmv, resulting in about 2–3 ‰ deviation for the d-excess. An assessment of the robustness of our findings shows overall reproducible behaviour over up to two years for different dry gas supplies, while being independent of the method for generating the water vapour, and to first order of the evaluation sequence. We propose to replace univariate mixing ratio dependency corrections by a new combined isotope composition–mixing ratio dependency correction. Using aircraft and ship-based measurements in an Arctic environment, we illustrate a relevant application of the correction. Based on our findings, we suggest that the dependency on the isotope composition may be primarily related to spectroscopy. Repeatedly characterising the combined isotope composition–mixing ratio dependency of laser spectrometers when performing water vapour measurements in the Arctic, at high elevation, or on aircraft, appears critical for enabling reliable data interpretation in dry environments.

1 Introduction

Stable water isotopes (hydrogen and oxygen) are natural tracers in the atmosphere and hydrosphere, and have long been used to improve our understanding of the hydrological cycle and climate processes (Dansgaard, 1953, 1954; Gat, 1996). Advances in laser spectroscopy now allow high frequency in situ measurements of the isotope composition of water vapour in the atmosphere (Kerstel, 2004; Kerstel and Gianfrani, 2008). One commercially available type of instrument is the Cavity Ring–Down Spectrometer (CRDS) manufactured by Picarro Inc., USA. The measurement principle of CRDS is based upon the

absorption of a laser pulse at a wavelength specific to a given isotopologue (O'Keefe and Deacon, 1988; Crosson, 2008). The L2130-i and L2140-i CRDS analysers have an optimal performance within a water vapour mixing ratio of $19'000 \sim 21'000$ ppmv (parts per million by volume), where high signal-to-noise ratios enable precise measurements. This range is typically maintained during liquid sample analysis. In situ measurements of the atmospheric water vapour isotopes are not constrained to this optimal mixing ratio range (Gupta et al., 2009). At lower water vapour mixing ratios, the measurement uncertainty increases due to weaker absorption, and thus lower signal-to-noise ratios. Additionally, outside of this range, the measurement suffers from a mixing ratio-dependent deviation of the isotope composition. Since atmospheric mixing ratios can vary from below 500 ppmv in dry regions (e.g., polar regions or the middle and upper troposphere) to $30'000$ ppmv or more in humid regions (e.g., tropics), an appropriate correction to this *mixing ratio dependency* for high-quality in situ measurements of atmospheric water vapour is required (e.g., Aemisegger et al., 2012; Bonne et al., 2014).

The water vapour mixing ratio dependency (hereafter *mixing ratio dependency*), sometimes also named humidity–isotope response (Steen-Larsen et al., 2013, 2014) or concentration dependency (Wen et al., 2012; Bailey et al., 2015) of infrared laser spectrometers for water isotopes has been described in numerous studies (e.g., Lis et al., 2008; Schmidt et al., 2010; Sturm and Knohl, 2010; Bastrikov et al., 2014; Sodemann et al., 2017). Many studies found the mixing ratio dependency to be nonlinear and to some extent specific to both the instrument used and the isotope composition measured. For example, reviewing the then available systems for vapour generation on a Picarro L1115-i and L1102-i, Wen et al. (2012) showed that the mixing ratio dependency could vary for each specific instrument. Aemisegger et al. (2012) demonstrated that the mixing ratio dependency varies for different instrument types and generations, and is affected by the matrix gas used during calibration. However, these authors did not find a substantial impact of the isotope composition when testing four different standards. Bonne et al. (2014) speculated that the different mixing ratio dependency functions at low mixing ratios (below $2'000$ ppmv) for their two working standards are likely an artefact of residual water vapour after using a molecular sieve. Bailey et al. (2015) found mixing ratio dependency to be clearly different for three tested standard waters, while emphasizing the uncertainty from statistical fitting where the characterisation data are infrequent. Sodemann et al. (2017) found a substantial impact of a mixing ratio dependency correction when processing aircraft measurements of d-excess over the Mediterranean, but did not account in detail for different isotopic standards. Bonne et al. (2019) characterised the mixing ratio dependency of their ship-based water vapour isotope measurements using four water standards, noting a dependency of the mixing ratio dependency on isotope standard. They did not observe a significant drift for the dependency for measurements separated by several months. Using the ambient air dried through an indicating drierite as carrier gas, Thurnherr et al. (2019) characterised the mixing ratio dependency for their customized L2130-i analyser operating with two different cavity flow rates. They observed a moderate dependency on the isotope composition with a normal cavity flow rate ($\sim$50 sccm) but a much weaker or negligible dependency on the isotope composition with a high cavity flow rate ($\sim$300 sccm).

To summarize, only some previous studies have recognised the impact of the isotope composition of measured standards on the mixing ratio dependency as a significant uncertainty source. More importantly, so far no systematic investigation of the influence of the isotope composition on the mixing ratio dependency has been conducted. Given the potentially large impact of such corrections at very low water vapour mixing ratios, this is an important piece required for enabling the reliable

interpretation and comparison of measurements at dry conditions, such as the Arctic, high elevation regions, or from research aircraft.

Here we present a systematic analysis of the impact of the isotope composition on the mixing ratio dependency for three commercial CRDS analysers, one Picarro L2130-i and two Picarro L2140-i, using five standard waters with different isotope compositions. Methods and data are presented in Sec. 2. Using the measurements from one analyser, we demonstrate the characterisation of the isotope composition–mixing ratio dependency in Sec. 3. We then evaluate the robustness of the isotope composition–mixing ratio dependency across the three analysers, considering as well the different vapour generators, matrix gas compositions, measuring sequences, and temporal stability (Sec. 4). A new correction scheme is proposed in Sec. 5. Using water vapour isotope measurements from aircraft and ship acquired during the IGP measurement campaign in the Iceland-Greenland Seas (Renfrew et al., 2019) as a test case, we investigate in Sec. 6 the potential impact of the isotope composition–mixing ratio dependency correction. We then discuss the potential sources of the dependency of the mixing ratio dependency on the isotope composition (Sec. 7). Finally, we provide recommendations on how to apply the correction scheme to other analysers (Sec. 8).

2 Methods and data

This section introduces the terminology used throughout the manuscript, the measurement principle of the used instruments, and provides an overview of the total 15 experiments (Table 1) that have been conducted to evaluate the potential influencing factors on the isotope composition–mixing ratio dependency separately and repeatedly. These 15 experiments can be separated into five categories with respect to their aims (Table 3). With these five categories, we assess influencing factors including the dependence on vapour generating method, the dependence on the specific instrument, the long term stability of the dependence behaviour, the influence from dry gas matrix and the influence from the measuring sequence. In the end, we introduce the in situ measurement data that are used to illustrate the impact of correction.

2.1 Terminology

The abundance of stable water isotopes in a reservoir is quantified as the concentration ratio of the rare ($HD^{16}O$ or $H_2^{18}O$) to the abundant isotopologue ($H_2^{16}O$). Note that the definition here is referred as molecular isotope ratio, as measured by laser spectrometry. This definition can be shown to be equal in first-order to the atomic isotope ratio determined by mass spectrometry (Mook et al., 2001). The (molecular) isotope ratio of hydrogen in a water reservoir, for example, is then:

$$^2R = \frac{[HD^{16}O]}{[H_2^{16}O]}. \quad (1)$$

Isotope abundance is generally reported as a deviation of the isotope ratio of a sample relative to that of a standard, known as δ value, and commonly expressed in units of per mil (‰) deviation from Vienna standard mean ocean water (VSMOW2; ~~$^2R_{VSMOW2} = 155.76 \pm 0.05 \times 10^{-6}$ (Hagemann et al., 1970) and $^{18}R_{VSMOW2} = 2005.20 \pm 0.45 \times 10^{-6}$~~ $^2R_{VSMOW2} = (155.76 \pm 0.05) \times 10$ (Hagemann et al., 1970) and $^{18}R_{VSMOW2} = (2005.20 \pm 0.45) \times 10^{-6}$ (Baertschi, 1976)) distributed by the International Atomic

Energy Agency (IAEA, 2009):

$$\delta = \frac{R_{\text{sample}} - R_{\text{standard}}}{R_{\text{standard}}} \cdot 1000\,‰. \tag{2}$$

The magnitude of the deviation introduced by the mixing ratio dependency is typically at least one order of magnitude less than the span of the isotope compositions of the measured standards. To focus on the deviation of the measured isotope compositions at various mixing ratios (δ_{meas}) from the isotope composition at a reference mixing ratio (δ_{cor}), we use the $\Delta\delta$ notation, which is defined as:

$$\Delta\delta = \delta_{\text{meas}} - \delta_{\text{cor}}. \tag{3}$$

We choose $20'000$ ppmv as reference level, within the nominal optimal performance range of the CDRS analyser. The isotope composition at the exact value of $20'000$ ppmv is thereby obtained by a linear interpolation between the closest measurements above and below $20'000$ ppmv (mostly between $19'000$ and $21'000$ ppmv). Note that all mixing ratios reported in this study are direct (raw) measurements from the CRDS, and that the isotope–mixing ratio dependency correction is applied to raw data before calibration.

While $\Delta\delta^{18}$O and $\Delta\delta$D are given directly by the definition above, the deviation for the secondary parameter d-excess $= \delta\text{D} - 8 \cdot \delta^{18}\text{O}$ (Dansgaard, 1964) is obtained from calculation: $\Delta d\text{-excess} = \Delta\delta\text{D} - 8 \cdot \Delta\delta^{18}\text{O}$.

2.2 Instruments

The instruments investigated in this study include two Picarro L2140-i (serial numbers HKDS2038 and HKDS2039) and one Picarro L2130-i (serial number HIDS2254) (all from Picarro Inc, Sunnyvale, USA). Hereafter, we refer to each instrument with their serial number. The instruments record at a data rate of $\sim$1.25 Hz and with a air flow of ~ 35 sccm through the cavity. To minimize instrument drift and errors from the spectral fitting, these CRDS systems precisely control the pressure and temperature of their cavities to be at ~~80 ± 0.02 °C and 50 ± 0.1 Torr~~ (80 ± 0.02) °C and (50 ± 0.1) Torr ((66.66 ± 0.13) hPa).

For the spectral fitting, the instruments target three absorption lines of water vapour in the region 7199–7200 cm^{-1} (Steig et al., 2014). In CRDS, a laser saturates the measurement cavity at one of the selected absorption wavelengths. After switching the laser off, a photodetector measures the decay (ring–down) of photons leaving the cavity through the semi–transparent mirrors (slightly less than 100% reflectivity). The ring–down time is inversely related to the total optical loss in the cavity. For an empty cavity, the ring–down time is determined solely by the reflectivity of the mirrors. For a cavity containing gas that absorbs light, the ring–down time will be shorter due to the additional absorption from the gas. The absorption intensity at a particular wavelength can be determined by comparing the ring–down time of an empty cavity to the ring–down time of a cavity that contains gas. The absorption intensities at all measured wavelengths generate an optical spectrum, where the height or underlying area of each absorption peak is proportional to the concentration of molecule that generated the signal. The height or underlying area of each absorption peak is calculated based on the proper fitting of the absorption baseline. At lower water vapour concentrations, the signal-to-noise ratio decreases, and fitting algorithms are affected by various error sources (see Sec. 7).

As a custom modification, the L2130-i with serial number HIDS2254 operates with two additional lasers, that allows for rapid switching between the three target wavelengths, enabling a higher (5 Hz) data acquisition rate, and a larger cavity flow rates than a regular L2130-i. In the present study, we used the flow rates and measurement frequency as for regular L2130-i analysers. The L2130-i use peak absorption for the spectral fitting, whereas the L2140-i uses an integrated absorption within the spectral features (Steig et al., 2014). The L2140-i is therefore substantially less sensitive to pressure broadening and narrowing of the absorption lines, for example due to changes in the matrix gas which can affect older–generation analysers, such as the L2120-i (Johnson and Rella, 2017). Manufacturer specifications commonly state a measurement range for vapour of $1'000$ to $50'000$ ppmv. As a custom modification, all instruments used here have been calibrated by the manufacturer down to 200 ppmv with a not further specified procedure.

Water vapour measurements with these instruments have a total error budget that involves the uncertainty from the calibration standards projecting onto the VSMOW2–SLAP2 scale, and from the time averaging employed on the native time resolution data. The Allan deviation quantifies the precision depending on averaging time interval. Previous studies found typical Allan deviations < 0.1 ‰ for δ^{18}O, and ~ 0.1 ‰ for δD at $15'700$ ppmv for averaging times of 1–2 min for the L2130-i (Aemisegger et al., 2012), and similar values for these averaging times for the L2140-i (Steig et al., 2014). Any corrections for the mixing ratio dependency are applied to the raw data at native time resolution. The uncertainty of any correction is thereby given by a combination of the averaging time of the vapour measurements at a given mixing ratio, and the uncertainty of the employed calibration standards.

2.3 Standard waters

To identify the influence of the isotope composition on the mixing ratio dependency, we have used multiple internal standard waters calibrated on the international VSMOW2–SLAP2 scale to characterise the mixing ratio dependency. The standard waters include four laboratory standards in use at Facility for Advanced Isotopic Research and Monitoring of Weather, Climate and Biogeochemical Cycling (FARLAB), University of Bergen and three laboratory standards in use at the Isotope Laboratory of University of Iceland (UI) (Table 2). For the FARLAB standards, one is obtained from snow in Greenland (GSM1), one made of mountain snow from Norway (VATS), one that consists of deionised tap water at Bergen (DI) and one made of evaporated DI water (EVAP). Besides the four laboratory standards, we have also used an even mixing between GSM1 and VATS (named MIX) and the uncalibrated deionised tap water (TAP). For the UI standards, one is from snow at NEEM ice core drilling site in Greenland (NEEM), one consists of groundwater in Reykjavik (GV) and one made of Milli-Q purified water based on ocean water from Bermuda (BERM). The isotope compositions of all the used waters span from -33.52 to 5.03 ‰ for δ^{18}O, and from -262.95 to 6.26 ‰ for δD (Table 2).

2.4 Vapour generation methods

We use two methods to generate vapour for characterising the isotope composition–mixing ratio dependency of the three instruments, namely discrete liquid injections and continuous vapour streaming. These are essentially two ways of generating

a vapour sample to be analysed by the infrared spectrometers. Both methods involve injection of a liquid standard water into a heated evaporation chamber where the injected water is completely evaporated and mixed with a dry matrix gas.

2.4.1 Dry gas supply

Previous studies for Picarro CRDS analysers preceding the L2140-i show that the matrix gas has an influence on the characterisation of mixing ratio dependence on the CRDS isotope measurement of water vapour (Aemisegger et al., 2012; Johnson and Rella, 2017). It is therefore important to know the influence of the matrix gas on the isotope composition–mixing ratio dependency to determine a preferred method for obtaining the final correction relationship depending on the measurement situation. The manufacturer recommends a customer-supplied gas drying unit (e.g. Drierite desiccants) to supply dry gas for the SDM unit. Here, we either used a single drying unit with ambient air, or dry gas cylinders that contain synthetic air (synthetic air 5.5, purity 99.9995 %, Praxair Norge AS) or N_2 (Nitrogen 5.0, purity $>$ 99.999 %, Praxair Norge AS). We have tested the three types of dry gas supply with the characterisation on instrument HIDS2254 for continuous vapour streaming and characterised the three analysers using synthetic air and/or N_2 for discrete liquid injections. Ambient air dried through Drierite can still contain some moisture (typically about 200 ppmv when the ambient water vapour is around 10′000 ppmv), which can contribute a non-negligible fraction to the measured isotope composition at low mixing ratios (e.g., 10 % below 2′000 ppmv). The use of several drying units in a row, vertical arrangement of drying units to prevent preferential gas flow and careful handling of tubing tightness may provide the same background mixing ratio as with a gas cylinder (Kurita et al., 2012), but has not been tested here.

2.4.2 Discrete liquid injections

The discrete liquid injections repeatedly generate vapour pulses by injecting between 0-2μl of standard water from 1.5 ml PTFE/rubber-septum sealed vials with a 10 μl syringe (VWR, Part No.: 002977). Injections are operated by an autosampler (A0325, Picarro Inc, USA) or by manual injection. Vaporisation of liquid water is achieved within a Picarro vaporiser (A0211, Picarro Inc, USA) set to 110 °C. The vaporiser mixes the water vapour with synthetic air or N_2 from a gas cylinder at a pressure set to ~~$\sim$ 2.5 psi~~$\sim$ 170 hPa. The vaporiser chamber seals off for a few seconds to allow sufficient mixing between vapour and the matrix gas, before delivering the mixture to the analyser at a highly stable mixing ratio.

Each time before switching to a new standard water, 8–12 injections of the new standard water at a mixing ratio of $\sim$ 20′000 ppmv were applied to account for memory effects from the previous injections. Then the sequence begins from the lowest ($\sim$ 500 ppmv) and ends at the highest ($\sim$ 23′000 ppmv) mixing ratio. Various mixing ratios are obtained by adjusting the injection volume in the 10 μl syringe. Injection volume was modified to be between 0.05 and 2.5 μl with a step of 0.05 μl, resulting in mixing ratios between approximately 500 and 23′000 ppmv with a step of $\sim$ 450 ppmv. Four injections in high precision mode (longer measurement period, approximate 10 min per injection) were applied at each mixing ratio, and the last three injections were then averaged for further analysis. Injections with an injection volume of 2 μl ($\sim$ 19′000 ppmv) were carried out at the beginning and end of a sequence to account for potential instrument drift. A sequence for one standard water approximately lasts 35 hours. The instrument drift within a sequence has typically a magnitude of ~~0.05 ± 0.02~~ (0.05 ± 0.02)

‰, ~~0.7 ± 0.1~~ (0.7 ± 0.1) ‰ and ~~0.4 ± 0.1~~ (0.4 ± 0.1) ‰ for δ^{18}O, δD and d-excess, respectively. The drift is 4–7 times larger than the uncertainty associated with the estimated drift but one order smaller than the deviation introduced by the mixing ratio dependency; it is corrected by assuming a temporal linearity during the sequence period.

Manual liquid injections were carried out during a field deployment where no autosampler was available. During manual injections, it is challenging to maintain a constant injection volume, and thus difficult to achieve precise control of water vapour mixing ratios. In this case, only injection volumes between 0.2 and 1.6 μl with a step of ~ 0.2 μl are employed, roughly corresponding to mixing ratios between $2'400$ and $24'000$ ppmv with a step of $\sim 3'000$ ppmv. Despite the shorter measurement period (about 6 hours), the instrument drift within a sequence increased by a factor of 2–3 for δ^{18}O (~~0.16 ± 0.03~~ (0.16 ± 0.03) ‰) and δD (~~1.65 ± 0.18~~ (1.65 ± 0.18) ‰), resulting in a drift of ~~0.37 ± 0.22~~ (0.37 ± 0.22) ‰ for d-excess. The relatively high instrument drift compared to the autosampler injections in the laboratory is most likely due to the uncertainty introduced by the variable injection volume, and the operation on a container on the deck of a research vessel (Renfrew et al., 2019). Instrument drift is corrected by assuming linear drift during each characterisation experiment. In all characterisation experiments, we applied three to five FARLAB standard waters when using an autosampler, or three UI standard waters in the case with manual injections.

2.4.3 Continuous vapour streaming

To test the influence of the vapour generation method, we used continuous water vapour streaming of two laboratory standard waters (DI and GSM1). A continuous vapour stream is generated via a so-called standard delivery module (SDM, A0101, Picarro Inc, USA). The SDM is a device with two syringe pumps, that provides automated delivery of two standard waters at up to three water concentrations per standard. The standard water is delivered to the Picarro vaporiser, where the standard water is instantly vaporised at 140 °C and simultaneously mixed with a dry matrix gas. The routines for vapour streaming at different mixing ratios applied here follow recommendations by the manufacturer to characterise each instrument's mixing ratio dependency (SDM user manual, Picarro Inc). Mixing ratios between 600 ppmv and $24'000$ ppmv were obtained by adjusting liquid water injection speed of the syringe pumps from 0.002 $\mu l\, s^{-1}$ to 0.8 $\mu l\, s^{-1}$. The generated standard vapour is continuously delivered to and measured by the spectrometer. During the characterisation, we measured a total of about 25 mixing ratios at a step of $\sim 1'000$ ppmv (0.003 $\mu l\, s^{-1}$) for each standard water. Each mixing ratio is measured for 20–40 minutes and the averaged value of a 5 minutes period close to the end of the measurement is used in the analysis. Due to unstable calibration performance, only 1–2 min long sections were used for the characterisations done in July 2016 and Feb 2018 for the laboratory standard DI on instrument HIDS2254.

A measurement sequence of standard GSM1 with ambient air dried through Drierite shows that the magnitude of the instrument drift during a 22 hour measurement with the SDM is similar to that of the liquid injection with an autosampler. However, due to the lower precision with the SDM measurement, the instrument drift is comparable (~~0.10 ± 0.09~~ (0.10 ± 0.09) ‰ and ~~0.96 ± 0.36~~ (0.96 ± 0.36) ‰ for δ^{18}O and δD respectively) or smaller (~~0.24 ± 0.78~~ (0.24 ± 0.78) ‰ for d-excess) compared to the uncertainty associated with the estimated drift. Therefore, except for the measurement with standard GSM1 above, the measurements with the SDM are not corrected for instrument drift.

2.5 In situ measurement data for studying the impact of the isotope composition–mixing ratio dependency correction

In order to test the impact of the isotope composition–mixing ratio dependency correction on actual measurements, we applied the proposed correction scheme to two datasets obtained from in situ vapour measurements during the Iceland Greenland Seas Project (Renfrew et al., 2019) in March 2018 onboard a research aircraft (analyser HIDS2254) and a research vessel (analyser HKDS2038) in the Iceland-Greenland Seas ($\sim 68°$N;12°W).

The analyser HIDS2254 was installed onboard a Twin Otter research aircraft. The instrument was fixed on a rack on the right side of the non-pressurized cabin. A 3.5 m stainless steel tube with $3/8$ inch diameter, insulated and heated to 50 °C, was leading from a backward facing inlet located behind the right cockpit door to the analyser. A rearward-facing inlet was selected to ensure that only vapour (and not particles or droplets) would be sampled. A manifold pump was used to draw the vapour through the inlet at a flow rate of about 8 slpm. The HIDS2254 was taking a sub-sample through a 0.2 m stainless steel tubing in low-flow mode at a flow rate of ~ 35 sccm. The selected vapour measurements from the aircraft were taken in the lower troposphere above the Iceland sea during a Cold Air Outbreak (CAO) on March 4, 2018. The particular water vapour measurement segment utilized here was taken during a 9 min long descent of the aircraft from $2'900$ m a.s.l. to 180 m a.s.l. A Greenland blocking associated with northerlies in the Greenland-Iceland Seas caused cold atmospheric temperatures, with an average of -12 °C at altitudes below 200 m. Accordingly, mixing ratios at low levels were ranging from $2'000$ to $2'700$ ppmv. At higher levels, mixing ratios were as low as about 900 ppmv. After applying any correction schemes (see below), the water vapour isotope data from the aircraft are calibrated to the VSMOW2-SLAP2 scale using the long-term average of calibrations with internal FARLAB laboratory standards GSM1 and DI using the SDM before and after the flight survey (details described in a forthcoming publication).

For the vapour measurements onboard the research vessel (R/V Alliance), the analyser HKDS2038 was installed inside a heated measurement container which was placed on the crew deck at about 6 m above the water surface. The ambient air was drawn into the container with a flow rate around 8 slpm by a manifold pump through a 5 m long 1/4 inch stainless steel tube, heated to about 50 °C by self-regulating heating tape. The tube inlet was mounted 4 m above the boat deck, protected from precipitation with a downward facing tin can. The selected time period from the research vessel was acquired during a CAO event between March 14 and 16, 2018. At the beginning of the event, the mixing ratio dropped from $6'000$ to below $3'000$ ppmv within 2 hours then stayed around $3'000$ ppmv for about 24 hours before it increased again to $8'000$ ppmv.

3 Isotope composition–mixing ratio dependency

In this section we present the isotope composition–mixing ratio dependency from the characterisation result for instrument HIDS2254 (Fig. 1). The characterisation is carried out using the method of discrete liquid injections (experiment 1). At each mixing ratio, in total four injections in high precision mode are carried out, and the last three injections are averaged for further analysis. The uncertainty at each mixing ratio is calculated as the standard deviation of the three taken injections; this standard deviation (color error bars in Fig. 1) is substantially smaller than the standard deviation of one single injection (indicated as thick grey error bars in Fig. 1).

The mixing ratio dependency for δ^{18}O, displayed as the deviation $\Delta\delta^{18}$O, exhibits a skewed, inverse U-shape (Fig. 1a) for all of the water standards. As an example, standard GSM1 (dark blue symbols) starts with a deviation of -0.1 ‰ for a high mixing ratio of $23'000$ ppmv, becomes positive after passing $20'000$ ppmv, continues to increase until reaching a maximum around $3'000$ ppmv. Then $\Delta\delta^{18}$O quickly drops at lower mixing ratios, and becomes negative again around 500 ppmv. As the mixing ratio further decreases, the magnitude of the deviation increases substantially. Notably, the mixing ratio dependencies of the other four standard waters (light blue, green, orange, and red symbols for MIX, VATS, DI and EVAP, respectively) also depict an inverse U-shape. However, the maxima become smaller and shift towards higher mixing ratios (bottom right in Fig. 1a) with more enriched isotope composition. This isotope-composition-related shift leads to an enlarged difference of $\Delta\delta^{18}$O between any the standard waters. For example, $\Delta\delta^{18}$O for GSM1 (dark blue symbols) and EVAP (red symbols) differs by ~ 0.9 ‰ at $2'000$ ppmv, and by 2.0 ‰ at $1'000$ ppmv.

The isotope-composition-related shift is even more pronounced for $\Delta\delta$D (Fig. 1b). For the standard waters with relatively depleted isotope compositions (GSM1, dark blue and MIX, light blue), $\Delta\delta$D is positive and becomes larger as mixing ratios decrease. For the standard waters with relatively enriched isotope compositions (VATS, green; DI, orange; EVAP, dark red), $\Delta\delta$D becomes more negative with decreasing mixing ratios. This leads to an increasing divergence of the mixing ratio dependency at $\sim 15'000$ ppmv and below. For example, $\Delta\delta$D for GSM1 (dark blue) and EVAP (red) differ by ~ 11 ‰ at $2'000$ ppmv, and by ~ 21 ‰ at $1'000$ ppmv.

The isotope-composition dependency of $\Delta\delta^{18}$O and $\Delta\delta$D have a substantial impact on the mixing ratio dependency of Δd-excess for different water standards. The mixing ratio dependency of Δd-excess below $\sim 15'000$ ppmv now exhibits a U-shape, with the minimum located between $4'000$ (DI, orange) and $7'000$ ppmv (GSM1, dark blue). The deviation for GSM1 (dark blue) and EVAP (red) differs by ~ 3.8 ‰ at $2'000$ ppmv, and by ~ 5.3 ‰ at $1'000$ ppmv.

In summary, this characterisation shows that the mixing ratio dependency varies systematically according to the isotope composition of the measured standard water. It is most pronounced at low mixing ratios (below $10'000$ ppmv) and increases at lower mixing ratios. The substantial deviations are clearly important for in situ water vapour measurements in dry environments, in particular when the water vapour has large variations in the isotope composition. As is demonstrated in Sect. 4, we find that this systematic isotope composition–mixing ratio dependency is irrespective of water vapour generation method and dry gas supply, and exists in similar form in all three CRDS spectrometers characterised here.

The mixing ratio dependency of the HIDS2254 seems to vary systematically with the isotope composition of the water standards, suggesting a potential spectroscopic origin (Sec. 7). This isotope composition–mixing ratio dependency will not be sufficiently removed by a uniform correction based on a single water standard alone. However, the dependency can be corrected for if we can establish a correction function that takes both the mixing ratio and the isotope composition into account. First we investigate how robust and stable over time the described isotope dependency is, before proposing a correction framework based on our characterisation results.

4 Robustness and temporal stability of the isotope composition–mixing ratio dependency

We carefully analysed the robustness of the isotope composition–mixing ratio dependency with respect to the choice of the method for vapour generation, the dry gas supply, the measuring sequence, individual instruments and instrument type, and its stability over time using in total 15 experiments (Table 1). Here we provide a summary of the results from these different experiments, with the detailed results given in Appendix A.

The robustness test indicates that the isotope composition–mixing ratio dependency is consistent across the two tested vapour generation methods, i.e., discrete liquid injections and continuous vapour streaming (Appendix A1; Fig. A1a-c). Characterisations with synthetic air and N_2 are in agreement for δD, but deviate for δ^{18}O (Appendix A2, Fig. A1d-f). A particularly substantial disagreement is found for the experiment using Drierite. This is likely caused by the contribution from water vapour remaining in the matrix air after the drying unit. The measuring sequence from high to low mixing ratios, or reverse, shows great similarity in the results, indicating that the potential hysteresis effects are not substantial (Appendix A3, Fig. A1g-i). However, we do note a different result for δ^{18}O at the lowest mixing ratio during one of the repeated experiments using MIX water (not shown). We suspect that the high sensitivity of the isotope composition–mixing ratio dependency at this range of δ^{18}O values could lead to pronounced deviations. While this aspect deserves further attention, we consider it as second–order regarding to the existence and cause of an isotope composition–mixing ratio dependency in the investigated CRDS instruments. Tests of all three analysers with discrete autosampler injections and N_2 as matrix gas show a similar isotope composition–mixing ratio dependency in all three investigated analysers (Appendix A4; Fig. A2). The repeated characterisation of analysers HIDS2254 and HKDS2038 during an up to 2-year time period show that the isotope composition–mixing ratio dependency is an instrument characteristic that is to first order constant over time (Appendix A5, Fig. A3).

In summary, the isotope composition–mixing ratio dependency is at first order robust across a range of key parameters, and stable over time. However, it is also apparent that individual instruments have a different strength and shape of the instrument characteristic, requiring individual correction. In the next sections, we apply and evaluate a new scheme to correct for the isotope composition–mixing ratio dependency.

5 Correction framework

We now use the characterisation result from instrument HIDS2254 obtained above as an example on how to derive a correction procedure for the isotope composition–mixing ratio dependency, following 6 sequential steps. Due to the systematic behaviour observed in Fig. 1, we chose a simple, traceable fitting procedure to obtain the two-dimensional correction function that can potentially be related to a physical cause. For the sake of simplicity, the equations in the following are formulated to be valid for both δ^{18}O and δD.

5.1 General formulation

1. We obtain the mixing ratio dependency for each water standard as raw (uncorrected, uncalibrated) measurements of the isotope compositions. The water standards thereby cover a wide range of isotope compositions, and different mixing ratios, in particular also at low mixing ratio.

2. We express the mixing ratio dependency for each water standard as the deviation of the raw measurements to the reference value at $20'000$ ppmv (Eq. (3)). The reference value is obtained by a linear interpolation between the closest measurements above and below $20'000$ ppmv. These deviations are denoted as $\Delta\delta^{18}$O, $\Delta\delta$D and Δd-excess as described in Sect. 2.1.

3. A suitable fitting function is fitted to the mixing ratio dependency of each standard water. Here we used fitting functions of the form

$$f_\delta(x) = \frac{a_\delta}{x} + b_\delta x + c_\delta, \tag{4}$$

where x is the mixing ratio, δ indicates the isotope composition of the standard waters, and a_δ, b_δ and c_δ are fitting coefficients for each water standard and isotope species.

4. We express the obtained fitting coefficients as a function of the isotope composition as $a(\delta)$, $b(\delta)$ and $c(\delta)$ for all the standard waters (Fig. 2, symbols). This reveals a dependency of the fitting coefficients on the isotope composition of the water standard. We now fit a suitable function to this dependency, here using a quadratic polynomial:

$$\begin{cases} a(\delta) = m_a(\delta - n_a)^2 + k_a, \\ b(\delta) = m_b(\delta - n_b)^2 + k_b, \\ c(\delta) = m_c(\delta - n_c)^2 + k_c, \end{cases} \tag{5}$$

where δ is the isotope composition, and m, n and k are the respective fitting coefficients of the quadratic polynomials.

5. By replacing the parameters a_δ, b_δ and c_δ in Eq. (4) through their parametric expressions in Eq. (5), we obtain the generalized fitting for the mixing ratio dependency, which is a function of both the mixing ratio x, and the isotope composition of the measured water δ:

$$f(x,\delta) = \frac{a(\delta)}{x} + b(\delta)x + c(\delta). \tag{6}$$

6. Using Eq. (6), given any measured raw mixing ratio and isotope composition within the range investigated here, we can now correct the measured isotope compositions to a reference mixing ratio at $20'000$ ppmv. Thereby, the isotope composition at $20'000$ ppmv (δ_{cor}) is the unknown; its analytical solution is found from solving the equation

$$\delta_{\text{meas}} - \delta_{\text{cor}} = \frac{a(\delta_{\text{cor}})}{h} + b(\delta_{\text{cor}}) \cdot h + c(\delta_{\text{cor}}), \tag{7}$$

where h is the measured raw mixing ratio and δ_{meas} is the measured isotope composition at that mixing ratio. The right hand side of the equation is the isotopic deviation determined from Eq. (6). The coefficients $a(\delta_{\text{cor}})$, $b(\delta_{\text{cor}})$ and $c(\delta_{\text{cor}})$ are determined from Eq. (5). Eq. (7) is a quadratic function; the procedure to obtain its analytical solution is given in Appendix C.

5.2 Correction function for analyser HIDS2254

We now exemplify the general steps above for the analyser with serial number HIDS2254. The results from step 1 and 2 for HIDS2254 are presented in Sec. 3. Here we use a range from -33.07 to 5.03 ‰ for δ^{18}O and from -262.95 to 4.75 ‰ for δD, and mixing ratios between 500 and $25'000$ ppmv (experiment 1 in Table 1).

The coefficients a_δ, b_δ and c_δ obtained in step 3 from Eq. (4) for the five standard waters measured on instrument HIDS2254 are given in Table 4. While the magnitude differs between the coefficients, scaling analysis shows that each of the terms ($\frac{a}{x}$, bx and c) on the right hand side of Eq. (4) contributes similarly to the isotope composition–mixing ratio dependency (not shown). The fitting results from step 4 are shown in Fig. 1 (solid color line). The choice of this type of function captures the behaviour of the isotope composition–mixing ratio dependency for both $\Delta\delta^{18}$O and $\Delta\delta$D of each standard water. Hereby, the fit for Δd-excess is calculated from the fit of $\Delta\delta$ by $\Delta d\text{-excess}_{\text{fit}} = \Delta\delta\text{D} - 8 \cdot \Delta\delta^{18}\text{O}$.

The coefficients m, n and k obtained in step 4 in Eq. (5) are given in Table 5. The fitting results (solid line) with the fitting uncertainty (95 % confidence interval; black dotted line) are shown in Fig. 2. Since we only fit five data points, the fitting uncertainty is large, resulting in a relatively large standard deviation for the isotope composition deviations $\Delta\delta$. This large standard deviation for $\Delta\delta$ can be reduced by using a bootstrapping approach (Efron, 1979) to estimate the fitting uncertainty in Eq. (5) (Appendix B).

Following step 5, this results in a two-dimensional correction surface for each isotopologue as shown in Fig. 3 (black contours). For illustration purposes, some contours are omitted below $4'000$ ppmv for both δ^{18}O and δD. The isotope composition–mixing ratio dependency for both δ^{18}O and δD increase substantially at low mixing ratios. For δ^{18}O, the deviation changes from positive to negative as mixing ratio decreases below $\sim 4'000$ ppmv. For δD, the deviation increases below $10'000$ ppmv, and splits into both positive and negative contributions, depending on the isotope composition. The uncertainty (one standard deviation) for the deviation $\Delta\delta$ is typically one order of magnitude smaller than the $\Delta\delta$ values at the corresponding position.

The surface function exhibits the same features as determined from the experimental results, underlining that the fitting procedure reflects the main characteristics of the isotope composition–mixing ratio dependency from the experimental data. At $20'000$ ppmv, the correction function is not exactly zero, as the fit which is based on all measurements is not constrained to the point $[20'000, 0]$ ppmv. This deficiency could be addressed by a modified fitting procedure. Below 500 ppmv, the correction function has larger uncertainties due to the lack of measurements at this mixing ratio range. Note that the fitting functions used in Eq. (4) and Eq. (5) are purely phenomenological and do not result from a particular physical model. Still, we recommend the proposed parametrisation to characterise individual instruments.

6 Impact of the isotope composition–mixing ratio dependency correction

We now investigate the impact of the isotope composition–mixing ratio dependency correction in situ measurements of the isotope composition of water vapour with two CRDS analysers installed onboard a research aircraft (HIDS2254), and a research vessel (HKDS2038, see Sec. 2.5).

6.1 Impact on the aircraft measurements

Low water vapour mixing ratios and a relatively wide range of (depleted) isotope compositions make water vapour isotope measurements from a research aircraft particularly suitable for demonstrating the impact of the new isotope composition–mixing ratio dependency correction. Fig. 4 shows a vertical profile of one-minute averaged water vapour isotope measurements above the Iceland Sea (Sec. 2.5). During the descent of the aircraft from $2'900$ m a.s.l to minimum safe altitude, the water vapour mixing ratio gradually increases from about 800 ppmv at the top to $2'300$ ppmv near the surface (Fig. 4d). The stable isotope profiles (Fig. 4a-c) show three main characteristics. Above about $2'000$ m a.s.l., δ^{18}O and δD are depleted (~ -42 ‰ and -320 ‰), with *d*-excess between 10 and 20 ‰. Between $2'000$ and $1'400$ m a.s.l., there is a transition where δ^{18}O and δD increase to around -30 ‰ and -240 ‰ respectively, and *d*-excess decreases to ~ -5 ‰. Below $1'400$ m a.s.l., δ^{18}O, δD and *d*-excess gradually increase until reaching about -22 ‰, -170 ‰ and 8 ‰, respectively near the surface. The uncertainty (one standard deviation) of the profile is obtained using the uncertainty propagation law, including the uncertainty (one standard deviation) of the one-minute averaged dataset (here the dominating source of uncertainty), and the uncertainty of the correction scheme.

First, we investigate the impact of the new correction scheme introduced here. This correction, abbreviated as *iso-hum-corr*, modifies the uncorrected dataset in the region above $2'000$ m a.s.l. by about -0.4 ‰ and -13.3 ‰ for δ^{18}O and δD, respectively, resulting in a change of about -10.4 ‰ for *d*-excess (Fig. 4, red circles vs. black dots). The impact of applying the new correction scheme on the aircraft measurements can be understood by examining where the dataset align in the correction surface function (Fig. 3, red crosses). For both δ^{18}O and δD, the aircraft dataset which is characterised with low mixing ratio and depleted isotope compositions clusters in the left bottom corner of the surface function. This is the most sensitive area of the correction, causing thus the largest deviations in the surface function.

To assess the benefit of the new isotope composition–mixing ratio dependency correction, we take this new correction scheme as the reference scheme and compare its impact to three other correction schemes. The first scheme corrects only for mixing ratio dependency based on standard DI (*hum-corr-DI*, Fig. 4, orange crosses). The second correction follows the same procedure but is based on standard GSM1 (*hum-corr-GSM1*, Fig. 4, blue squares), and the third correction follows an approach proposed by Bonne et al. (2014) for in situ vapour measurements in southern Greenland. Instead of correcting the mixing ratio dependency for the vapour measurements, the Bonne et al. (2014) approach corrects the mixing ratio dependency for the calibration standards. Thus, assuming the mixing ratio dependencies of the two employed standards remain stable during the measurement period, the measured isotope compositions of these two standards are corrected using the mixing ratio dependency function to the ambient air mixing ratio of each single vapour measurement. Then, the linear regression computed

from these two corrected standard measurements against their certified values is applied to calibrate the vapour measurement to VSMOW2-SLAP2 scale. This scheme is hereafter referred as *2-std-hum-corr* (Fig. 4, green triangles).

The different correction schemes modify the uncorrected dataset differently. The δ^{18}O profile is only marginally affected by the correction below $1'400$ m a.s.l. (Fig. 4a). For the measurements above $1'400$ m a.s.l., differences become more pronounced, but are masked by large uncertainty as the aircraft was descending through a strong mixing ratio gradient. At elevations above $2'000$ m a.s.l., all corrections show clear deviations, and we focus our comparison at this region. The *hum-corr-DI* stands out with a positive correction of about 0.8 ‰, while the other three schemes induce a negative correction of between -0.3 and -0.7 ‰. The δD profile exhibits a similar pattern, but with more apparent differences between the correction schemes (Fig. 4b). This results in an even more pronounced correction in the *d*-excess profile (Fig. 4c).

The impact of applying the correction scheme using single standard water (thus accounting for only mixing ratio dependency) relies on the choice of the used standard water. Using the correction *hum-corr-DI* introduces the largest deviation (1.1 ‰, 18.3 ‰ and 9.5 ‰, for δ^{18}O, δD and *d*-excess, respectively), while using the correction *hum-corr-GSM1* produces results much closer to that of the reference scheme (with an offset of 0.1 ‰ and 4.2 ‰ for δ^{18}O and δD, respectively and 3.4 ‰ for *d*-excess). For this specific aircraft measurement (where the surface condition is already quite dry during cold air outbreak event) the isotope composition of standard GSM1 happens to closely resemble the average isotope composition of the measurement. However, in the case of a previously unknown range of isotope compositions, or strongly varying conditions, a comprehensive characterisation of mixing ratio dependency with multiple standard waters can provide advantages and should be preferred. Unknown ranges are particularly likely for atmospheric measurements of vertical profiles in humid regions (e.g., tropics and subtropics), or over a wide area from moving platforms.

Finally, applying the alternative calibration approach used in Bonne et al. (2014) (*2-std-hum-corr*) results in only slightly more depleted isotope values than the reference, with an offset of about -0.3 ‰ and -0.5 ‰ for δ^{18}O and δD, respectively, resulting in a change of 1.7 ‰ for *d*-excess. The small discrepancy between the *2-std-hum-corr* and *iso-hum-corr* is mainly due to the following three factors. Firstly, depending on the number of the used standard waters, the interpolation scheme for the isotopic deviations in between those of the used standard waters can be different. *2-std-hum-corr* makes use of the mixing ratio dependency functions of only two standard waters. In this way the deviations can only be linearly interpolated between the two standard waters. In contrast, by measuring five standard waters, the reference scheme is able to account for non-linearities during interpolation. Secondly, *2-std-hum-corr* corrects the two standard waters to the mixing ratio of the measurement while the reference scheme corrects the measurement to the mixing ratio of the two standard waters (i.e. the reference mixing ratio). Based on the mixing ratio dependency feature of the two standard waters, the choice of correcting the two standard waters will result in a higher slope for VSMOW2-SLAP2 calibration line. Consequently, the measurements after calibration are stretched to two ends, i.e., the measurements with the isotope composition close to that of standard DI become more enriched and those close to that of standard GSM1 become more depleted. Finally, the mixing ratio dependency functions for GSM1 and DI in *2-std-hum-corr* (using the individual fit for GSM1 or DI respectively) are not exactly identical to those used in the reference scheme (from the surface function determined by the measurements of five standard waters). Despite the small discrepancy, the consistent results of *2-std-hum-corr* with that of the reference scheme indicate that a correction scheme using the mixing ratio

dependency functions of only two standard waters covering the measured isotope composition range can work sufficiently well in certain situations.

6.2 Impact on the ship-based measurements

Applying the four different correction schemes to the ship-based measurement data has a much weaker impact on the corrected series of vapour measurement (not shown). After applying our isotope composition–mixing ratio dependency correction scheme, the uncorrected dataset changes on the order of 0.06 and 0.15 ‰ for δ^{18}O and δD, respectively, leading to a change on the order of -0.5 ‰ for *d*-excess. This is mainly because these ship measurements were carried out at the ocean surface with relatively high mixing ratios (from $2'500$ to $8'000$ ppmv), and less depleted isotope compositions (-23 to -12 ‰ for δ^{18}O and -160 to -100 ‰ for δD), compared to the aircraft measurements. As can be identified in Fig. 3, the ship data (blue dots) are located coincidentially in an area with low sensitivity in the correction surface. A linear interpolation between two standards may not capture such a saddle point correctly. This indicates that measurements are not under all conditions sensitive to the correction of the isotope composition–mixing ratio dependency. Ultimately, however, certainty about a reliable correction will only be achieved by a complete characterisation of the isotope composition and mixing ratios covered by the measurements.

7 Discussion

Our careful characterisation experiments show that the isotope composition–mixing ratio dependency affects measurements at low mixing ratios for all three investigated stable water isotope CRDS analysers. Here, we discuss possible causes of the isotope composition–mixing ratio dependency. In particular, we explore to what extent this dependency is an artefact from mixing with water remaining within the analyser, or an instrument behaviour resulting from spectroscopic effects.

7.1 Artefact from mixing

If we assume the dependency is a result from mixing with remnant water, there would be mainly two candidates of the background moisture source: (1) the remaining water vapour in the dry gas supply; (2) the remaining water vapour from previous measurements in the analyser. By changing the dry gas supply from the ambient air dried through Drierite to synthetic air or N_2 from cylinder which typically provides a dry gas with a mixing ratio below 10 ppmv, we can exclude the possible influence from the background moisture in the dry gas supply. In order to quantify the amount and the isotope compositions of the remaining water vapour from previous measurement, we have applied several successive, so called *empty injections* via the autosampler. Thereby, no liquid is injected, and only dry gas is flushed into the vaporiser. Results from these empty injections show that the remaining water vapour in the system typically has a mixing ratio of about 60–80 ppmv, with its isotope composition closely following those of the previous injections. If the mixing ratio dependency were a result of the mixing between the injected water and the remaining water vapour from previous measurement, by injecting the same standard water during a characterisation run, we would expect a mixing of two water vapour masses of the same isotope compositions at different mixing ratios. As a consequence, we would expect the mixed vapour to have the same isotope compositions, which is not the

case. Finally, the shape of the isotope composition–mixing ratio dependency with a maximum between $2'000$ and $6'000$ ppmv (Fig. 1a) is not consistent with the expectation of a memory effect that would monotonously increase with decreasing mixing ratio. The slight hysteresis observed during the upward/downward calibration runs indicates that there may be contributions from remnant water, for example on walls or filter surfaces in the analyzer, that only exchange once a sufficiently humid air-
5 mass is introduced into the analyzer. Such contributions do however appear to be of second–order compared to the substantial changes of the mixing ratio dependency with the isotope composition.

7.2 Spectroscopic effect

Now we explore the second hypothesis, namely that the isotope composition–mixing ratio dependency is an instrument be-
10 haviour resulting from spectroscopic effects. The manufacturer recommends a procedure for water vapour dependency calibration, using their SDM or similar device (Picarro, 2017), similar to what we have employed. While the first-order effect can be removed from a linear fit, there are second–order, non-linear components, that become more apparent the more the water concentration changes from the recommended range of operation ($5'000 - 25'000$ ppmv). In the following we discuss the potential reasons for the origin of the water vapour and isotope dependency from a spectroscopic standpoint based on the published literature (Steig et al., 2014; Rella et al., 2015; Johnson and Rella, 2017).

15 The two modules of CRDS analyser used in our experiments (i.e., Picarro L2140-i and L2140-i) target thee absorption lines of water vapour in the region 7199–7200 cm^{-1}, namely near 7199.960, 7200.135 and 7200.305 cm^{-1} for $H_2^{18}O$, $H_2^{16}O$ and $HD^{16}O$, respectively (Fig. 5). These absorption lines broaden or narrow, depending on the partial pressure of the gas mixture in the cavity, and can be affected by changes in their baseline due to other nearby strong absorption lines. A fitting algorithm then fits the measured absorption spectrum to an expected model spectrum and adjusts the model parameters in order to minimize
20 the residual error. Broadening/narrowing of lines due to changing gas mixture, and baseline shifts are particular challenges to the fitting algorithm (Johnson and Rella, 2017), and cause residuals during the fitting procedure, which induce instrument error.

The L2130-i and earlier spectrometers use the absorption peak as a free parameter in the fitting algorithm. The peak shape and thus the peak amplitude can suffer from the above mentioned broadening/narrowing effect, introducing potential error un-
25 der conditions of varying concentration or matrix gases. The fitting algorithms of the L2140-i spectrometers, in contrast, have a higher number of ring–downs due to a different strategy for obtaining laser resonance, using a different laser stabilisation scheme. This allows to fit the integrated absorption, rather than the peak amplitude, of each absorption line. Since the integrated absorption is a constant independent of pressure, the fitting is expected to be more accurate, with a low sensitivity to broadening/narrowing effects arising from changes of water concentrations and background gas compositions (Steig et al., 2014). One
30 part of the retrieval algorithm is the removal of the baseline from the $H_2^{16}O$ spectrum. To this end, changes in the baseline from nearby strong absorption lines as a result from concentration changes or cross-interference from other gas species is a possible source of error for either fitting algorithm. Other possible source of error can be absorption loss nonlinearities due to small imperfections of the instrument such as the non-zero shut-off time of the laser and response time of the ring–down detector

(Rella et al., 2015). Unless fitting algorithms take the actual line shapes into consideration directly, some residual effects are likely to persist.

The retrieval of H_2O concentration and the stable isotope compositions $\delta H_2^{18}O$ and $\delta HD^{16}O$ (identical to $\delta^{18}O$ and δD) is implemented similar to the procedure described for CH_4 and $\delta^{13}CH_4$ (Rella et al., 2015). Considering a linear dependency of absorption to concentration (which is not always true), where the mole fraction of $H_2^{18}O$ (c_{18}) is related to the absorption peak height α_{18} with a proportionality constant k_{18} and an error offset ϵ_{18}, we have:

$$c_{18} = k_{18}\alpha_{18} + \epsilon_{18}. \tag{8}$$

Note that the expressions above should apply to both the L2130-i and L2140-i spectrometers, with the only difference that the absorption peak height is replaced by the integrated absorption (Steig et al., 2014).

Based on the molecular definition of a delta value with respect to Vienna Standard Mean Ocean Water (VSMOW), and an isotope ratio of the sample ${}^{18}R = \frac{[H_2^{18}O]}{[H_2^{16}O]}$ and of VSMOW ~~${}^{18}R_{VSMOW} = 2005.20 \pm 0.45 \times 10^{-6}$~~ ${}^{18}R_{VSMOW} = (2005.20 \pm 0.45) \times 10^{-6}$ (Baertschi, 1976), we have:

$$\delta H_2^{18}O\ [\text{in } ‰] = 1000\left(\frac{{}^{18}R_{\text{sample}}}{{}^{18}R_{\text{VSMOW}}} - 1\right). \tag{9}$$

The retrieval can then be formulated as:

$$\delta H_2^{18}O = 1000\left(\frac{k_{18}\alpha_{18} + \epsilon_{18}}{(k_{16}\alpha_{16} + \epsilon_{16})R_{\text{VSMOW}}} - 1\right). \tag{10}$$

For an ideal spectrometer, the calibration coefficients are constants (i.e., $k_{18} = \kappa_{18}$ and $k_{16} = \kappa_{16}$) and the calibration offsets are zero (i.e., $\epsilon_{18} = \epsilon_{16} = 0$). These assumptions lead to the expected retrieval for a spectrometer as:

$$\delta H_2^{18}O = \frac{1000}{R_{\text{VSMOW}}}\frac{\kappa_{18}\alpha_{18}}{\kappa_{16}\alpha_{16}} - 1000. \tag{11}$$

The actual spectrometer is not ideal, but in most situations has a highly linear and stable performance (Rella et al., 2015). Nevertheless, it can be calibrated based on the linear dependency of $\delta H_2^{18}O$ to $\frac{\alpha_{18}}{\alpha_{16}}$, using a linear expression of the form:

$$\delta H_2^{18}O = A\frac{\alpha_{18}}{\alpha_{16}} + B, \tag{12}$$

where calibration constants A and B can be determined based on the measurable quantities $\delta H_2^{18}O$ and $\frac{\alpha_{18}}{\alpha_{16}}$ on a reference instrument in the factory. These determined calibration constants slightly deviate from the expected values in Eq. (11). They are then transferred from the reference instrument to each new instrument of the same type (Rella et al., 2015).

If Eq. (12) is used for calibration of the water analysers (not reported in the published literature), there are two potential sources of error. First, the dependencies on isotope ratio may not be entirely linear (even when assuming a linear relationship, the coefficient is not necessarily a constant and the offset not necessarily to be zero), and remain as residuals. Second, the change of this relationship with differing mixing ratio may remain unexplored. Furthermore, manufacturing tolerances will induce deviations from the reference instrument on which such an initial calibration has been carried out, and instruments have

therefore to be calibrated individually to obtain suitable post-processing methods. The initial instrument calibration procedure may therefore be one potential origin for the isotope composition–mixing ratio dependency identified here.

Deviations from an ideal spectrometer stem from the potential spectrometer errors due to small imperfections of the instrument. One possible error is the absorption loss offset that could occur when the baseline loss is not reproduced well by the fitting algorithm. This absorption offset then leads to a mole fraction offset, ϵ_{18} in Eq. (8). The measured $\delta H_2^{18}O$ including the effect of absorption offset can be formulated explicitly, following Rella et al. (2015) (their Appendix S1.1), as:

$$\delta H_2^{18}O = \frac{1000}{R_{VSMOW}} \left(\frac{k_{18}\alpha_{18}}{k_{16}\alpha_{16}} + \frac{\alpha_0}{\alpha_{16}} \right) - 1000, \tag{13}$$

where α_0 is the net absorption loss parameter, that should to first order be independent of water concentration and isotope ratio. Comparing to Eq. (11) for an ideal spectrometer, the additional term $\frac{\alpha_0}{\alpha_{16}}$ in Eq. (13) creates an inverse relationship with water concentration, and should be responsible for deviations from the ideal spectrometer that are most evident at low mixing ratios.

Another possible spectrometer error is the so–called absorption loss non–linearity, which describes effects due to a shorter or longer ring–down time than expected in the optimal range of operations. These effects can be included as additional terms, again following Rella et al. (2015) (their Appendix S1.2), by including a non–linear dependency of α_{18} on α_{16} (i.e., $\alpha_{18} \Rightarrow \alpha_{18} + \beta\alpha_{16} + \gamma\alpha_{16}^2$):

$$\delta H_2^{18}O = \frac{1000}{R_{VSMOW}} \left(\frac{k_{18}\alpha_{18}}{k_{16}\alpha_{16}} + \gamma\frac{k_{18}\alpha_{16}}{k_{16}} + \frac{\alpha_0}{\alpha_{16}} \right) + \left(\frac{1000}{R_{VSMOW}} \frac{k_{18}}{k_{16}}\beta - 1000 \right), \tag{14}$$

The calibration coefficients are thereby assumed constant. The non–linearities from spectral cross–talk between $H_2^{16}O$ and $H_2^{18}O$ or imperfections in the baseline removal of the $H_2^{16}O$ absorption spectrum are present in several terms; such effects require calibration of each individual instrument to account for. When written in this explicit form, it appears consistent with expectations that a systematic isotope–composition mixing ratio dependency may be detected from careful analyser characterisation. The equation can be further simplified:

$$\delta H_2^{18}O = A\frac{\alpha_{18}}{\alpha_{16}} + \Gamma c_{16} + \frac{c_0}{c_{16}} + B'. \tag{15}$$

The difference between Eq. (15) and Eq. (12) represents the deviation from an ideal spectrometer due to non-linearities from imperfections in the baseline removal and spectral cross-talk between $H_2^{18}O$ and $H_2^{16}O$, and can be denoted as:

$$\Delta\delta H_2^{18}O = \Gamma c_{16} + \frac{c_0}{c_{16}} + \text{Const.} \tag{16}$$

The dependency on water concentration (c_{16}) in Eq. (16) appears consistent with the mixing ratio dependency function (Eq. (7)) identified in our systematic investigation of three analysers, supporting the hypothesis of a spectrometric origin for the isotope–composition mixing ratio dependency.

A similar form of mixing ratio correction is applied to the ^{17}O measurements using L2140-i analyser in the study of Steig et al. (2014) (their Eq. (22)), where the integrated absorption area instead of peak amplitude is used to calculate the absorption loss and the cross-talk between $H_2^{18}O$ and $H_2^{16}O$ is modelled with a bilinear relationship. Steig et al. (2014) notes that the introduction of an integrated absorption detection leads to a substantially improved behaviour for the mixing ratio dependency

over the peak amplitude detection for $\delta^{18}O$, but not for δD, with the reason remaining unclear. It is also worth to note that their instrument has not been evaluated for the low mixing ratio range, which is in the focus of this manuscript. It may be possible that part of the identified isotope composition dependency of the mixing ratio dependency stems from the so far lacking systematic analysis of the low mixing ratio range of the analyser for this effect.

One aspect that is not addressed here, but may be valuable to consider further in the future, is the availability of analysers with higher flow rates of above 300 sccm, for example for use in research aircraft (Sodemann et al., 2017). Given recent indications that the flow rate affects the isotope–composition mixing ratio dependency (Thurnherr et al., 2019), forthcoming studies should explore the flow rate as an additional parameter. This requires that suitable methods to generate standard vapour at these higher flow rates are available.

8 Final remarks and recommendations

We have systematically investigated the mixing ratio dependency of water vapour isotope measurements for three commercially available infra–red cavity ring–down spectrometers. We found that the mixing ratio dependency varies with the isotope composition of the measured vapour. We define this behaviour as the isotope composition–mixing ratio dependency. The dependency is robustly identified across 3 similar analysers, regarding several first-order parameters, and found to be stable over time. Using the characterisation results of five standard waters on a Picarro L2130-i as an example, we propose a correction scheme for this isotope composition–mixing ratio dependency. Using such a correction scheme, we can correct the isotopic measurements for any measured mixing ratio and isotope composition within the range investigated here.

To demonstrate the impact of the mixing ratio dependency correction, we have compared the proposed correction scheme with other published correction schemes, using in situ measurements from dry environments. The impact is found to be most substantial on the measurements at the low mixing ratios. Applying a correction scheme accounting for only mixing ratio dependency relies on the choice of the used standard water. For an aircraft dataset, using the mixing ratio dependency function based on the standard DI produces a large deviation from our proposed scheme; using the mixing ratio dependency based on standard GSM1 produces results similar to our proposed scheme, since it is closer to the average isotope composition of the aircraft dataset. Finally, we have investigated the impact of applying a correction scheme used by Bonne et al. (2014). This approach produces results in good agreement with that from our approach. The small discrepancy is due to the interpolation scheme (linear or non linear) of the isotopic deviation, the choice of correcting mixing ratio dependency of the standards or that of the vapour measurement and the small discrepancy in the mixing ratio dependency functions of the two standards. The consistent results indicate that a correction scheme using the mixing ratio dependency functions of only two standards covering the isotope composition could be sufficient if the correction surface can be sufficiently approximated by linear interpolation. Using ship measurements made at higher mixing ratio conditions, we find a weaker impact from the different correction schemes.

Given the non-monotonous characteristics of the isotope composition–mixing ratio dependency, we consider memory effects (i.e. mixing with water vapour from previous injections in the analyser) unlikely to be the dominanting factor. This renders

a spectroscopic origin as the most likely cause, possibly resulting from imperfections of the fitting algorithm at low water concentrations, or non-linearities in the fitting procedures (Rella et al., 2015).

The correction for the isotope composition–mixing ratio dependency is most relevant for in situ vapour isotope measurements where the ambient mixing ratio is low (below $4'000$ ppmv) and the isotope composition of measured vapour spans a large range. At higher mixing ratios, the investigated CRDS analysers show negligible dependency on either the mixing ratio or the isotope composition. If the isotope composition of ambient vapour varies in a small range during the sampling period, a simpler correction scheme could be employed, using the mixing ratio dependency of two or even one suitable standard water with a similar isotope composition as that of ambient vapour.

Based on our conclusions above, we recommend to identify the isotope composition–mixing ratio dependency for all Picarro CRDS analysers used for in situ water vapour isotope measurements, in particular when the low mixing ratio conditions are encountered.

If the measurements of multiple standard waters are not available, the approach used in Bonne et al. (2014) could be applied as an alternative correction approach. Their approach can produce similar results as that from the approach proposed here, but requires the characterisation of the mixing ratio dependency of two carefully selected calibration standards in a linear range of the correction surface. If the isotope composition of the ambient vapour varies only within a small range during the sampling period, such as during measurements close to the ocean surface, it may be sufficient to correct for the mixing ratio dependency using one standard water that has a similar isotope composition as that of the ambient vapour.

Our study is presently limited by the range of the standard waters used here (about $-33 \sim 5\,‰$ and $-263 \sim 5\,‰$ for δ^{18}O and δD, respectively). Depending on the measurement environment, more depleted or enriched standards would be needed to derive a correction function over the entire measurement range of samples potentially encountered during atmospheric measurements. With all standards being close to the global meteoric water line (GMWL), one aspect that will likely be missed here is the potential cross–interference between δ^{18}O and δD (Chris Rella, pers. comm., 2020). Identifying such cross interference can be relevant for applications where vapour samples deviate substantially from the GMWL, such as from geothermal vapour sources. One potential approach to identifying such cross–interferences could be to repeat the present analysis with spiked water standards, that deviate substantially from the GMWL.

Another limitation of the characterisations performed here is the substantial time demand. The characterisation method with liquid injections provides relatively high precision performance but requires an autosampler and takes about 1–2 weeks for four standard waters. The characterisation method with the SDM can be automated more easily, but requires manual intervention to apply more than two standards. A device that could provide any desired isotope composition and a given mixing ratio would be needed to fully automate the isotope composition–mixing ratio dependency of the instruments tested here.

A reproducible and accepted characterisation method is of utmost importance for comparing measurements across disparate locations and in bottom–up networks, in particular in the polar regions, and appears as a prerequisite for detecting representative signals in the stable isotope record on a regional scale. In particular studies employing the d-excess as an indicator of moisture origin or other tracer applications are therefore likely to profit from a detailed characterisation of their analysers according to our characterisation procedure, either before, during or after field deployments.

Data availability. Data used in the generation of the figures is attached as a supplement to this article.

Appendix A: Robustness and temporal stability

Here we detail the experiments conducted to assess the robustness of the isotope composition–mixing ratio dependency with regard to the vapour generation method, the dry gas supply, the measurement sequence, the individual analyser and analyser type, and with respect to temporal stability.

A1 Vapour generation method

To investigate whether the isotope composition–mixing ratio dependency is influenced by the choice of vapour generation method, we compare the characterisation result from discrete liquid injections and the SDM for instrument HIDS2254 (experiment 2 and 6; Fig. A1a-c). The same standard waters (GSM1 and DI) and dry gas supply (synthetic air) are used in the two experiments. The measurement using the SDM usually has a higher uncertainty since the continuous vapour streaming does not provide entirely constant mixing conditions, and the vapour stream can become unstable due to clogging and bubbles in the capillary. Overall, the results from the two vapour generation methods exhibit consistent dependency behaviours. However, discrepancy exists. For $\Delta\delta^{18}$O, there is an offset of 0.2–0.5 ‰ for DI between $1'000$ and $6'000$ ppmv. Inconsistency appears for GSM1 measurement below $2'000$ ppmv (Fig. A1a). For $\Delta\delta$D, the mixing ratio dependencies determined by the SDM method exhibit a slightly weaker dependency for both standard waters (Fig. A1b).

It is interesting to mention that the result of the discrete liquid injections in Feb 2017 (experiment 1; Fig. 1) depicts a better agreement with that of the SDM in experiment 6 (comparison figure not shown). This indicates that the discrepancy in the results of the two vapour generation methods could be due to the small instrument drift as well as the high measurement uncertainty at lower mixing ratios.

Experiments using N_2 as dry gas supply (experiment 3 and 8) also gives a similar isotope composition–mixing ratio dependency between the two vapour generation methods (not shown), confirming that the isotope composition–mixing ratio dependency does not depend substantially on either of the two tested methods.

A2 Influence of dry gas supply

Next, we investigate whether the type of the dry gas supply has an influence on the characterisation results. To this end, we test the characterisation method via the SDM on instrument HIDS2254 with a supply of synthetic air, a supply of N_2 and a supply of dried ambient air through Drierite (experiment 6–8). The synthetic air and N_2 are tested with two standard waters (GSM1 and DI), and the Drierite is tested with one standard water (GSM1).

For mixing ratio dependency on δ^{18}O, the measurement with Drierite disagrees strongly from those with synthetic air and N_2 (Fig. A1e). As mixing ratio decreases below about $7'000$ ppmv, the measured GSM1 with Drierite exhibits a fast increasing positive deviation while that with synthetic air or N_2 exhibits a rather flat dependency. The measurements with synthetic air and N_2 show a largely similar shape. A small discrepancy exists below $15'000$ ppmv, where the two standard waters measured with

N_2 exhibit a small negative offset (~ 0.5 ‰). The mixing ratio dependencies on δD from all three types of the dry gas supply are in good agreement, despite a small (< 1.5 ‰) offset between the measurement with synthetic air and that with N_2 (Fig. A1e). The calculated *d*-excess follows the shape of δ^{18}O, with a different behaviour between the measurement with Drierite and those with synthetic air and N_2 below about $7'000$ ppmv (Fig. A1f). The *d*-excess of the experiment with N_2 exhibits a small positive offset (~ 0.5 ‰) compared to that of measurement with synthetic air. Overall, characterisation results with synthetic air and N_2 exhibit a mixing ratio dependency in a good agreement for the two investigated standard waters (GSM1 and DI). However, the characterisation result (for GSM1) with the Drierite differ significantly in δ^{18}O and thus *d*-excess.

The characterisation method of liquid injections via an autosampler is also tested with synthetic air and N_2. Again, the results exhibit a similar isotope composition–mixing ratio dependency from the two types of dry gas supply, despite a small discrepancy for δ^{18}O of GSM1 below $2'000$ ppmv and a relatively larger offset (0.5–1.3 ‰) for δ^{18}O of DI below $10'000$ ppmv (not shown). A test of synthetic air from a gas cylinder and dried ambient air from Drierite in the study of Aemisegger et al. (2012) also shows that the mixing ratio dependency for δ^{18}O is different while being more similar for δD. The observed discrepancy in the δ^{18}O deviation is possibly due to changes in the baseline of the spectrum around the $^1H_2^{18}O$ and $^1H_2^{16}O$ absorption peak, caused by slight differences in trace gas composition (Aemisegger et al., 2012; Rella et al., 2015).

A3 Influence from the measuring sequence

Finally, we investigate whether a measuring sequence with ascending or descending mixing ratio sequence influences mixing ratio dependency characterisation. The mixing ratio dependencies of GSM1, MIX and DI tap water characterised with ascending and descending mixing ratio sequences are shown in Fig. A1(g-i). For both $\Delta\delta^{18}$O and $\Delta\delta$D (Fig. A1g, h), the results from the two measuring sequences are in good agreement for all three waters, indicating that the influence from measuring sequence is minor. Though, there is a slightly detectable weaker mixing ratio dependency for the descending mixing ratio sequence (e.g., $\Delta\delta$D for GSM1 and DI). One possible explanation for the slightly weaker dependency at descending sequence is the memory effect from previous injections, e.g., some remaining water molecules would stick to the inner wall of the system (even after flushing the system with 12 injections at $20'000$ ppmv) and still play a role during the characterisation measurements. If this is the case, the measurements from descending mixing ratio sequence (starting with injections of higher mixing ratios at the beginning) would help to replace the remaining molecules by molecular exchange and therefore is more likely to represent the true dependency behaviour. Nonetheless, the good agreement between the two measuring sequences indicates that the potential hysteresis effects if any are not substantial. The resulting mixing ratio dependencies for Δd-excess (Fig. A1i) overall exhibit an increasing positive deviation towards the low mixing ratios, except for one mixing ratio step of MIX and two mixing ratio steps of GSM1. This underlines the high sensitivity of *d*-excess measurements due to the increasing uncertainty of δ^{18}O and δD values at very low mixing ratios.

It is worth to note that we have repeated three experiments for MIX (only results from one of the experiments is shown here). For one of the three experiments (not shown), the measurements for MIX below $2'000$ ppmv exhibit an interesting contrast in $\Delta\delta^{18}$O. The measurement at the lowest mixing ratio (around 500 ppmv) has constrained the mixing ratio dependency into slightly opposite directions. The contrast is not well understood. It is possible that this contrast stems from the fitting

uncertainties due to the lacking constraining points at the low end of mixing ratios. The contrast is not observed for the repeated experiment with added mixing ratio steps (Fig. A1g, green). It is also possible that for a standard whose isotopic composition is close to a turning point in the correction surface (Sect. 5), hysteresis effects with opposing sign may become visible within the range of uncertainty. This can be also found, for example, in the small shift of dependency shape in δD for VATS among the three analysers (Fig. A2b, e, h, green curve). Further tests with more in-between standards or a vapour generation approach that does not suffer from memory is needed to address this uncertainty in the dependency shape.

A4 Variations among CRDS analysers

To investigate the variations of the mixing ratio dependency between the individual instruments, we have repeated the same characterisation on three analysers (experiment 3, 9 and 14). The characterisation is carried out with four standard waters (GSM1, VATS, DI and EVAP), using liquid injections via an autosampler with N_2 as the mixing dry gas.

The characterisation results for the three analysers are shown in Fig. A2. For $\Delta\delta^{18}$O, the positive deviation for GSM1 below $4'000$ ppmv on instrument HKDS2038 is about 0.2–1.8 ‰ stronger than those on the other two analysers (Fig. A2a, d, g, blue). The mixing ratio dependency of VATS below $4'000$ ppmv is nearly flat on instrument HKDS2038 while exhibiting a substantial negative deviation on the other two analysers. The mixing ratio dependencies for the other two standard waters (DI and EVAP) are in good agreement among the three analysers. For $\Delta\delta$D, the mixing ratio dependency of VATS below $2'000$ ppmv is slightly positive on instrument HKDS2038 while being nearly flat on the other two analysers (Fig. A2b, e, h, green). The mixing ratio dependency for the other three standard waters (GSM1, DI and EVAP) agree well among the three analysers. The calculated *d*-excess (Fig. A2c, f, i) shows an increasing positive deviation towards the low end of mixing ratio for almost all the standard waters measured on the three analysers, except for DI and GSM1 measured on instrument HKDS2038, whose mixing ratio dependencies appear to be rather flat or even slightly negative.

Despite of the minor difference in the magnitude of the deviations, it is clear that the isotope composition–mixing ratio dependency exists in all three analysers investigated here. The behaviour of dependency is to the first order in good agreement across the analysers. For the standard waters with relatively depleted isotope compositions, the measurements on all the three analysers exhibit a mixing ratio dependency where the isotopic value increases as the mixing ratio decreases. For the standard waters with relatively enriched isotope compositions, the measurements exhibit a reversed mixing ratio dependency.

A5 Long-term stability

To quantify the long term stability of the isotope composition–mixing ratio dependency, we examine the temporal change of the fitting coefficients (a_δ, b_δ and c_δ) in Eq. (4). Figure A3 shows the fitting coefficients for the mixing ratio dependency characterised by liquid injections on instrument HIDS2254 in February 2017 (black line, experiment 1) and in May 2018 (red line, experiment 2). For the characterisation in May 2018, only four standard waters are measured; this results in a fit with a relatively large 95 % confidence interval. In this context, the change over time is considered insignificant if the coefficients (and their fitted curve) from the characterisation in May 2018 is within the 95 % confidence bounds for the fitted curve from the characterisation in February 2017.

For the mixing ratio dependency on δ^{18}O, the change of coefficient a is insignificant. However, it is worth to note that the fitting coefficient a with respect to standard GSM1 (Fig. A3a, the first data point) changes slightly from negative to positive. This small change results in an opposite mixing ratio dependency shape at low mixing ratio. The change of the mixing ratio dependency for GSM1 reflects partly on the sensitivity of the instrument on a certain range of isotope compositions and partly on the uncertainty arising from both low instrument precision and lack of measurements at low mixing ratios. The changes of coefficients b and c are substantial for the standard waters of relatively high δ^{18}O (Fig. A3b, c). A less negative b and a less positive c reflects a weaker mixing ratio dependency in May 2018. For the mixing ratio dependency on δD, reasonable agreement exhibits for all three fitting coefficients (Fig. A3d, e, f); this points to the same basic shape of the mixing ratio dependency on δD after a 15 month period.

A repeated characterisation with standard water DI determined via the SDM in July 2016, February 2018 and June 2018 (experiment 4, 5 and 6) indicates that the mixing ratio dependency for standard water DI is still consistent after nearly two years (not shown). The mixing ratio dependencies of the three standard waters (GSM1, VATS and DI) determined by liquid injections via an autosampler (experiment 9 and 10) and the other three standard waters (NEEM, GV and BERM) via manual injections on instrument HKDS2038 (experiment 12 and 13) indicate a consistent isotope composition–mixing ratio dependency after a running of one year and one month, respectively (not shown). Overall, the stability tests indicate that the isotope composition–mixing ratio dependency of each analyser is to first order stable on a long term basis (1–2 years).

Appendix B: Fitting uncertainty estimated using a bootstrapping approach

Since we only have 5 available data points to fit in (5), the resulted 95 % confidence interval of the fit is relatively broad (black dotted line, Fig. 2). This broad confidence interval results in a relatively large standard deviation for the isotopic deviation ($\Delta\delta$). For example, the resulted standard deviation for $\Delta\delta$ at $2'000$ ppmv is about 0.20, 2.69 and 3.13 ‰ for δ^{18}O, δD and d-excess, respectively. To reduce this large standard deviation for $\Delta\delta$, we use a bootstrapping approach (Efron, 1979) to estimate the fitting uncertainty in Eq. (5).

The bootstrapping approach can be explained by considering for example the coefficient a. Firstly, for each individual observation of a, we generate $1'000$ random values under a normal distribution with the mean and standard deviation being those of each available observation. We obtain now five sets of $1'000$ random values since we have five a from five standard waters. Then, we sample one value from each set of the $1'000$ random values and fit those sampled five values using Eq. (5). Finally, we repeat this process $1'000$ times, thus obtain $1'000$ fits. The standard deviation of the $1'000$ fits is the standard deviation that is adopted here (blue dotted line, Fig. 2).

In this way, the standard deviations estimated for the coefficients a, b and c are lowered to about 15, 0.4×10^{-6} and 8×10^{-3} for δ^{18}O and 100, 3×10^{-6} and 0.1 for δD, respectively. This in turn substantially reduces the resulted standard deviation for $\Delta\delta$. For example, the standard deviation for $\Delta\delta$ at $2'000$ ppmv is reduced by a factor of 20, being about 0.01, 0.11 and 0.14 ‰ for δ^{18}O, δD and d-excess, respectively.

Appendix C: Analytical solution for δ_{cor}

In the following we derive the analytical solution for δ_{cor} in Eq. (7) at the reference mixing ratio (i.e. $20'000$ ppmv). The derivation applies for both δ^{18}O and δD.

The coefficients a(δ_{cor}), b(δ_{cor}) and c(δ_{cor}) are given according to Eq. (5):

$$\begin{cases} a(\delta_{\text{cor}}) = m_a(\delta_{\text{cor}} - n_a)^2 + k_a, \\ b(\delta_{\text{cor}}) = m_b(\delta_{\text{cor}} - n_b)^2 + k_b, \\ c(\delta_{\text{cor}}) = m_c(\delta_{\text{cor}} - n_c)^2 + k_c, \end{cases} \tag{C1}$$

Substitute Eq. (C1) into Eq. (7) and rearrange the terms, we get:

$$A\delta_{\text{cor}}^2 + B\delta_{\text{cor}} + C = 0, \text{ where } \begin{cases} A = \dfrac{m_a}{h} + m_b h + m_c, \\ B = 1 - \dfrac{2m_a n_a}{h} - 2m_b n_b h - 2m_c n_c, \\ C = \dfrac{m_a n_a^2}{h} + m_b n_b^2 h + m_c n_c^2 + \dfrac{k_a}{h} + k_b h + k_c - \delta_{\text{meas}}, \end{cases} \tag{C2}$$

Eq. (C2) is a quadratic equation with its only physical solution being:

$$\delta_{\text{cor}} = \frac{-B + \sqrt{B^2 - 4AC}}{2A}. \tag{C3}$$

The coefficients m, n and k are already obtained from the fits in Eq. (5). When given a measured mixing ratio, h, and the corresponding isotope composition, δ_{meas}, we can obtain the isotope composition at $20'000$ ppmv, δ_{cor}, according to the solution Eq. (C3).

Competing interests. The authors declare that no competing interests are present in this study.

Acknowledgements. We thank Iris Thurnherr, Franziska Aemisegger and Pascal Graf from the Institute for Atmospheric and Climate Sciences, ETH Zurich, Hans Christian Steen-Larsen and Sonja Wahl from the Geophysical Institute, University of Bergen, Jean-Lionel Lacour and Tomas Foldes, for valuable discussions. Thanks for Arny Erla Sveinbjornsdottir from the Isotope Laboratory of University of Iceland for providing the UI standard waters. Jarle Berntsen from the Department of Mathematics at University of Bergen is acknowledged for helping to identify a suitable fitting function. We are grateful to the scientists and other personnel who made the measurements during the Iceland-Greenland Seas campaign in 2018 possible. This publication received funding from the Research Council of Norway through Projects SNOWPACE (Contract no. 262710) and FARLAB (Contract no. 245907). We thank Chris Rella for providing valuable comments on our manuscript. We would also like to express our gratitude to the editor and the three anonymous reviewers whose valuable comments have significantly helped to improve the clarity of this manuscript.

References

Aemisegger, F., Sturm, P., Graf, P., Sodemann, H., Pfahl, S., Knohl, A., and Wernli, H.: Measuring variations of δ^{18}O and δ^{2}H in atmospheric water vapour using two commercial laser-based spectrometers: an instrument characterisation study, Atmos, Meas. Tech, 5, 1491–1511, 2012.

Baertschi, P.: Absolute18O content of standard mean ocean water, Earth and Planetary Science Letters, 31, 341–344, 1976.

Bailey, A., Noone, D., Berkelhammer, M., Steen-Larsen, H. C., and Sato, P.: The stability and calibration of water vapor isotope ratio measurements during long-term deployments, Atmospheric Measurement Techniques, 8, 4521–4538, https://doi.org/10.5194/amt-8-4521-2015, 2015.

Bastrikov, V., Steen-Larsen, H. C., Masson-Delmotte, V., Gribanov, K., Cattani, O., Jouzel, J., and Zakharov, V.: Continuous measurements of atmospheric water vapour isotopes in western Siberia (Kourovka), Atmospheric Measurement Techniques, 7, 1763–1776, https://doi.org/10.5194/amt-7-1763-2014, 2014.

Bonne, J.-L., Masson-Delmotte, V., Cattani, O., Delmotte, M., Risi, C., Sodemann, H., and Steen-Larsen, H.: The isotopic composition of water vapour and precipitation in Ivittuut, southern Greenland, Atmospheric Chemistry and Physics, 14, 4419–4439, 2014.

Bonne, J.-L., Behrens, M., Meyer, H., Kipfstuhl, S., Rabe, B., Schönicke, L., Steen-Larsen, H. C., and Werner, M.: Resolving the controls of water vapour isotopes in the Atlantic sector, Nature communications, 10, 1632, 2019.

Crosson, E. R.: A cavity ring-down analyzer for measuring atmospheric levels of methane, carbon dioxide, and water vapor, Applied Physics B-Lasers And Optics, 92, 403–408, 2008.

Dansgaard, W.: The abundance of O18 in atmospheric water and water vapour, Tellus, 5, 461–469, 1953.

Dansgaard, W.: The O18-abundance in fresh water, Geochimica et Cosmochimica Acta, 6, 241–260, http://www.sciencedirect.com/science/article/B6V66-488Y5HP-1V6/2/e7ca8aaef7549373eab07d45b525387c, 1954.

Dansgaard, W.: Stable isotopes in precipitation, Tellus, 16, 436–468, 1964.

Efron, B.: Bootstrap Methods: Another Look at the Jackknife, Annals of Statistics, 7, 1–26, 1979.

Gat, J. R.: Oxygen and hydrogen isotopes in the hydrologic cycle, Annual Review of Earth and Planetary Sciences, 24, 225–262, 1996.

Goldenstein, C. S., Miller, V. A., Spearrin, R. M., and Strand, C. L.: SpectraPlot.com: Integrated spectroscopic modeling of atomic and molecular gases, Journal of Quantitative Spectroscopy and Radiative Transfer, 200, 249 – 257, https://doi.org/https://doi.org/10.1016/j.jqsrt.2017.06.007, http://www.sciencedirect.com/science/article/pii/S0022407317302996, 2017.

Gupta, P., Noone, D., Galewsky, J., Sweeney, C., and Vaughn, B. H.: Demonstration of high-precision continuous measurements of water vapor isotopologues in laboratory and remote field deployments using wavelength-scanned cavity ring-down spectroscopy (WS-CRDS) technology, Rapid Communications In Mass Spectrometry, 23, 2534–2542, 2009.

Hagemann, R., Nief, G., and Roth, E.: Absolute isotopic scale for deuterium analysis of natural waters. Absolute D/H ratio for SMOW 1, Tellus, 22, 712–715, 1970.

IAEA: Reference Sheet for VSMOW2 and SLAP2 international measurement standards, 2009.

Johnson, J. E. and Rella, C. W.: Effects of variation in background mixing ratios of N2, O2, and Ar on the measurement of δ 18O–H2O and δ 2H–H2O values by cavity ring-down spectroscopy, 2017.

Kerstel, E.: Isotope ratio infrared spectrometry, in: Handbook of stable isotope analytical techniques, pp. 759–787, Elsevier, 2004.

Kerstel, E. and Gianfrani, L.: Advances in laser-based isotope ratio measurements: selected applications, Applied Physics B-Lasers And Optics, 92, 439–449, 2008.

Kurita, N., Newman, B. D., Araguas-Araguas, L. J., and Aggarwal, P.: Evaluation of continuous water vapor delta D and delta O-18 measurements by off-axis integrated cavity output spectroscopy, Atmospheric Measurement Techniques, 5, 2069–2080, https://doi.org/10.5194/amt-5-2069-2012, 2012.

Lis, G., Wassenaar, L., and Hendry, M.: High-precision laser spectroscopy D/H and 18O/16O measurements of microliter natural water samples, Analytical chemistry, 80, 287–293, 2008.

Mook, W. G., Gat, J. R., Meijer, H. A., Rozanski, K., Froehlich, K., et al.: Environmental isotopes in the hydrological cycle: principles and applications, in: Technical Documents in Hydrology, UNESCO, 2001.

O'Keefe, A. and Deacon, D. A.: Cavity ring-down optical spectrometer for absorption measurements using pulsed laser sources, Review of scientific instruments, 59, 2544–2551, 1988.

Picarro, I.: Calibration guide for Picarro analyzers, 2017.

Rella, C. W., Hoffnagle, J., He, Y., and Tajima, S.: Local- and regional-scale measurements of CH_4, $\delta^{13}CH_4$, and C_2H_6 in the Uintah Basin using a mobile stable isotope analyzer, Atmospheric Measurement Techniques, 8, 4539–4559, https://doi.org/10.5194/amt-8-4539-2015, https://www.atmos-meas-tech.net/8/4539/2015/, 2015.

Renfrew, I., Pickart, R., Våge, K., Moore, G., Bracegirdle, T., Elvidge, A., Jeansson, E., Lachlan-Cope, T., McRaven, L., Papritz, L., et al.: The Iceland Greenland Seas Project, Bulletin of the American Meteorological Society, 2019.

Schmidt, M., Maseyk, K., Lett, C., Biron, P., Richard, P., Bariac, T., and Seibt, U.: Concentration effects on laser-based $\delta^{18}O$ and $\delta^{2}H$ measurements and implications for the calibration of vapour measurements with liquid standards, Rapid Communications in Mass Spectrometry, 24, 3553–3561, 2010.

Sodemann, H., Aemisegger, F., Pfahl, S., Bitter, M., Corsmeier, U., Feuerle, T., Graf, P., Hankers, R., Hsiao, G., Schulz, H., et al.: The stable isotopic composition of water vapour above Corsica during the HyMeX SOP1 campaign: insight into vertical mixing processes from lower-tropospheric survey flights, Atmospheric Chemistry and Physics, 17, 6125–6151, 2017.

Steen-Larsen, H. C., Johnsen, S. J., Masson-Delmotte, V., Stenni, B., Risi, C., Sodemann, H., Balslev-Clausen, D., Blunier, T., Dahl-Jensen, D., Ellehoj, M. D., Falourd, S., Grindsted, A., Gkinis, V., Jouzel, J., Popp, T., Sheldon, S., Simonsen, S. B., Sjolte, J., Steffensen, J. P., Sperlich, P., Sveinbjornsdottir, A. E., Vinther, B. M., and White, J. W. C.: Continuous monitoring of summer surface water vapor isotopic composition above the Greenland Ice Sheet, Atmospheric Chemistry and Physics, 13, 4815–4828, https://doi.org/10.5194/acp-13-4815-2013, 2013.

Steen-Larsen, H. C., Sveinbjörnsdottir, A. E., Peters, A. J., Masson-Delmotte, V., Guishard, M. P., Hsiao, G., Jouzel, J., Noone, D., Warren, J. K., and White, J. W. C.: Climatic controls on water vapor deuterium excess in the marine boundary layer of the North Atlantic based on 500 days of in situ, continuous measurements, Atmospheric Chemistry and Physics, 14, 7741–7756, https://doi.org/10.5194/acp-14-7741-2014, 2014.

Steig, E., Gkinis, V., Schauer, A., Schoenemann, S., Samek, K., Hoffnagle, J., Dennis, K., and Tan, S.: Calibrated high-precision 17O-excess measurements using cavity ring-down spectroscopy with laser-current-tuned cavity resonance, Meas. Tech, 7, 2421–2435, 2014.

Sturm, P. and Knohl, A.: Water vapor $\delta^{2}H$ and $\delta^{18}O$ measurements using off-axis integrated cavity output spectroscopy, Atmospheric Measurement Techniques, 3, 67–77, 2010.

Thurnherr, I., Kozachek, A., Graf, P., Weng, Y., Bolshiyanov, D., Landwehr, S., Pfahl, S., Schmale, J., Sodemann, H., Steen-Larsen, H. C., Toffoli, A., Wernli, H., and Aemisegger, F.: Meridional and vertical variations of the water vapour isotopic composition in the marine boundary layer over the Atlantic and Southern Ocean, Atmospheric Chemistry and Physics Discussions, 2019, 1–40, https://doi.org/10.5194/acp-2019-782, https://www.atmos-chem-phys-discuss.net/acp-2019-782/, 2019.

Wen, X. F., Lee, X., Sun, X. M., Wang, J. L., Tang, Y. K., Li, S. G., and Yu, G. R.: Intercomparison of four commercial analyzers for water vapor isotope measurement, Journal of Atmospheric and Oceanic Technology, 29, 235–247, https://doi.org/10.1175/JTECH-D-10-05037.1, 2012.

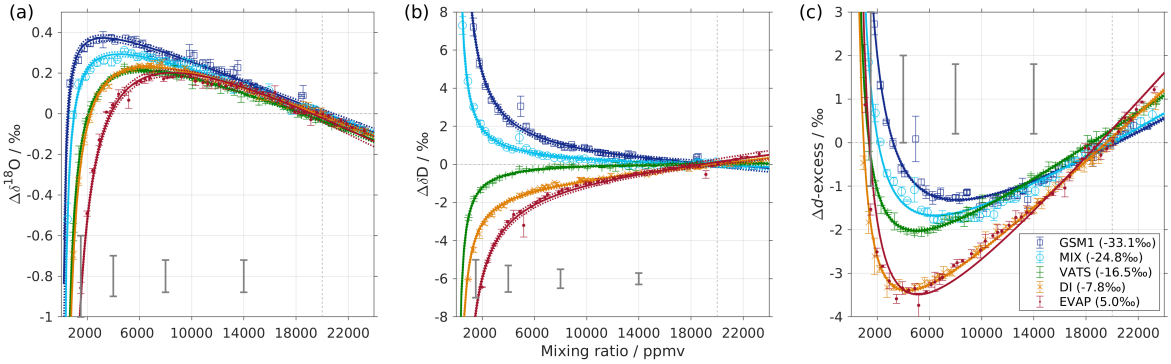

Figure 1. Mixing ratio dependency of uncalibrated measurements for **(a)**: δ^{18}O, **(b)**: δD and **(c)**: d-excess for five standard waters (GSM1, MIX, VATS, DI and EVAP) on instrument HIDS2254 (Picarro L2130-i) with discrete liquid injections via an autosampler (experiment 1). Mixing ratio dependency is expressed as the deviation Δ of the measured isotope composition at each mixing ratio with respect to the reference mixing ratio of $20'000$ ppmv. Symbol and error bar represents the mean and the standard deviation of the mean for the last three of total four injections at each mixing ratio. Solid lines are fits with the function $f(x) = \frac{a}{x} + bx + c$. Dashed lines are the 95 % confidence interval for the corresponding fit. Measurements and fits for d-excess are calculated from $\Delta d\text{-excess} = \Delta\delta\text{D} - 8 \cdot \Delta\delta^{18}\text{O}$. The typical one standard deviation of a single injection at the corresponding mixing ratio is indicated by grey error bars. Two outliers (at about $4'300$ and $8'900$ ppmv) are removed from GSM1 measurements and one outlier (at about $9'000$ ppmv) is removed from VATS measurements.

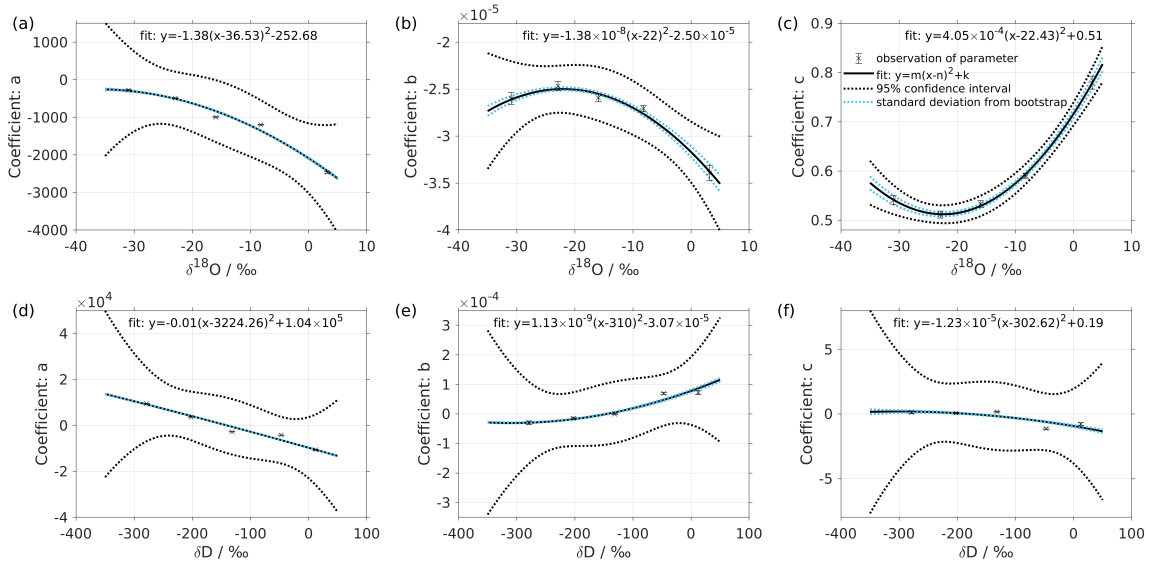

Figure 2. Dependency of fitting coefficients a, b and c on δ^{18}O **(a)–(c)** and on δD **(d)–(f)**. The coefficients a, b and c are from the fits for the five standard waters in Fig. 1. Solid line is the quadratic fit with $f_j(y) = m_j(y - n_j)^2 + k_j$. Black dotted line shows the 95 % confidence interval. Blue dotted line shows the standard deviation estimated from a bootstrapping method.

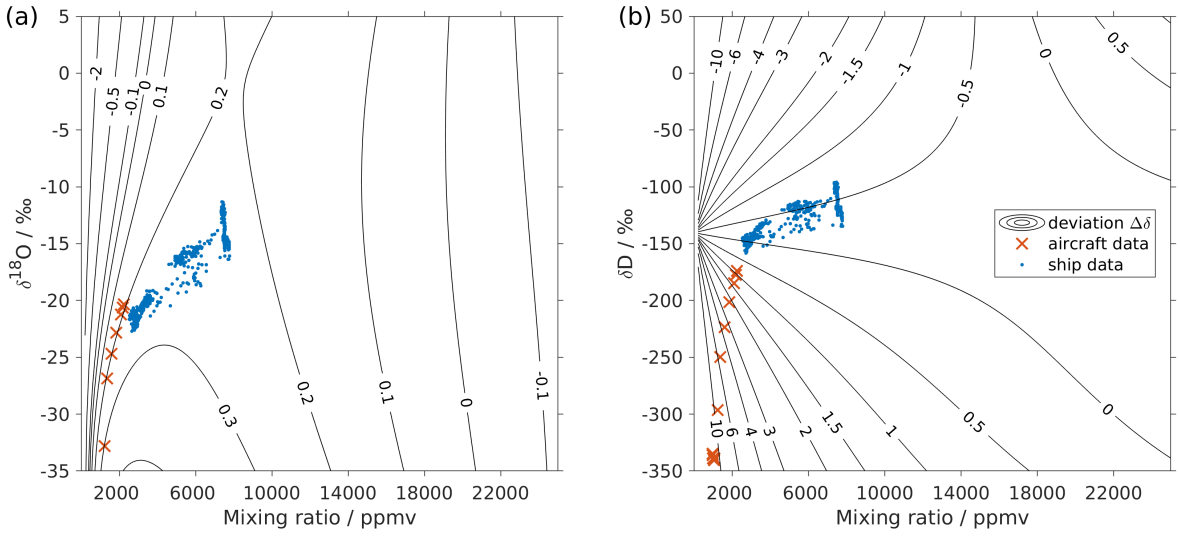

Figure 3. Surface function of the isotopic deviations for **(a)** δ^{18}O and **(b)** δD, based on the isotope composition–mixing ratio dependency of instrument HIDS2254 (Picarro L2130-i). The x-axis is the raw mixing ratio and y-axis shows the raw isotope composition at $20'000$ ppmv. Contours with numbers indicate the isotopic deviation, $\Delta\delta$. Symbols show the isotope measurements over the Iceland Sea: one min averaged measurements from an aircraft in the lower troposphere (red crosses) and measurements at 10 minutes resolution from a research vessel (blue dots). The measurements from the aircraft were done with instrument HIDS2254 (Picarro L2130-i) and those on the research vessel were done with instrument HKDS2038 (Picarro L2140-i).

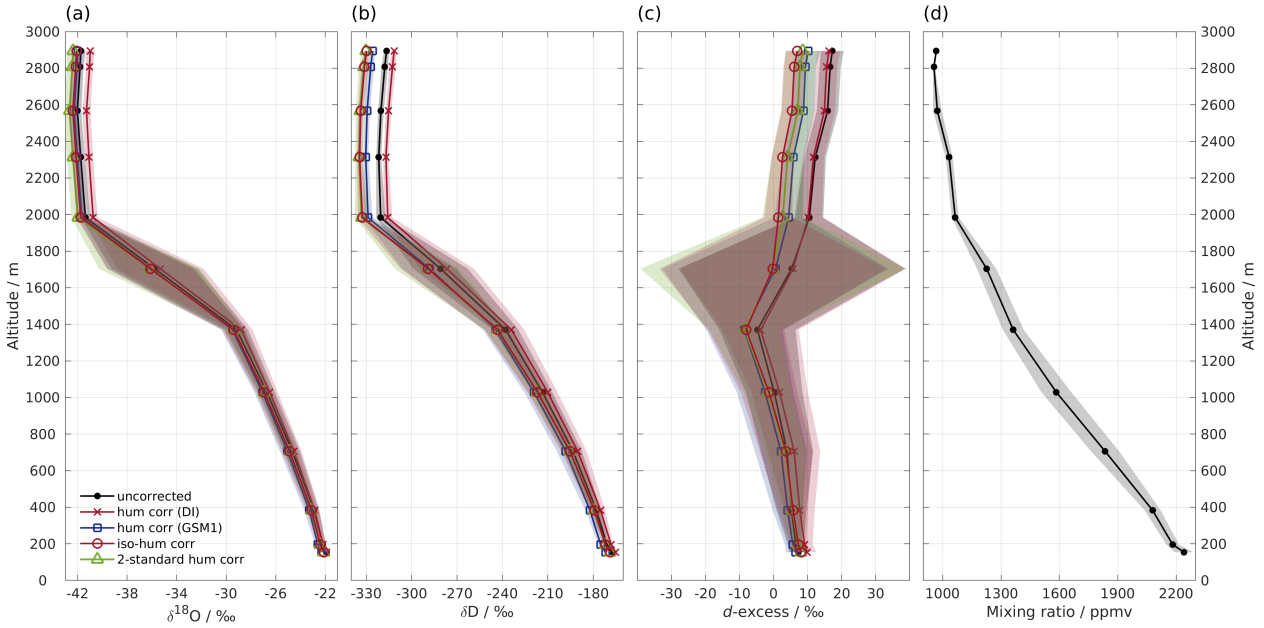

Figure 4. Vertical profiles of **(a)** δ^{18}O, **(b)** δD, **(c)** d-excess and **(d)** mixing ratio measured by instrument HIDS2254 on an aircraft above the Iceland Sea on Mar 04, 2018. Shown are one min averaged profiles of the uncorrected dataset (black line with dot) and four datasets using different isotope composition–mixing ratio dependency correction schemes: using the mixing ratio dependency of standard DI (orange curve with cross), standard GSM1 (blue curve with square), the isotope composition–mixing ratio dependency surface function (red curve with circle), and using two mixing ratio-dependency-corrected standards (green curve with triangle). All the datasets are calibrated to VSMOW2-SLAP2 scale. Shading shows the total uncertainty (one standard deviation) for the corresponding profiles. Note that the profile of δD has been adjusted 30 s forward to account for the longer response time of molecular HD^{16}O. The large uncertainty between $1'400$ and $2'000$ m for d-excess is partly due to the rapid evolution of δ^{18}O and δD profiles and partly due to the dephasing between δ^{18}O and δD profiles caused by different response time.

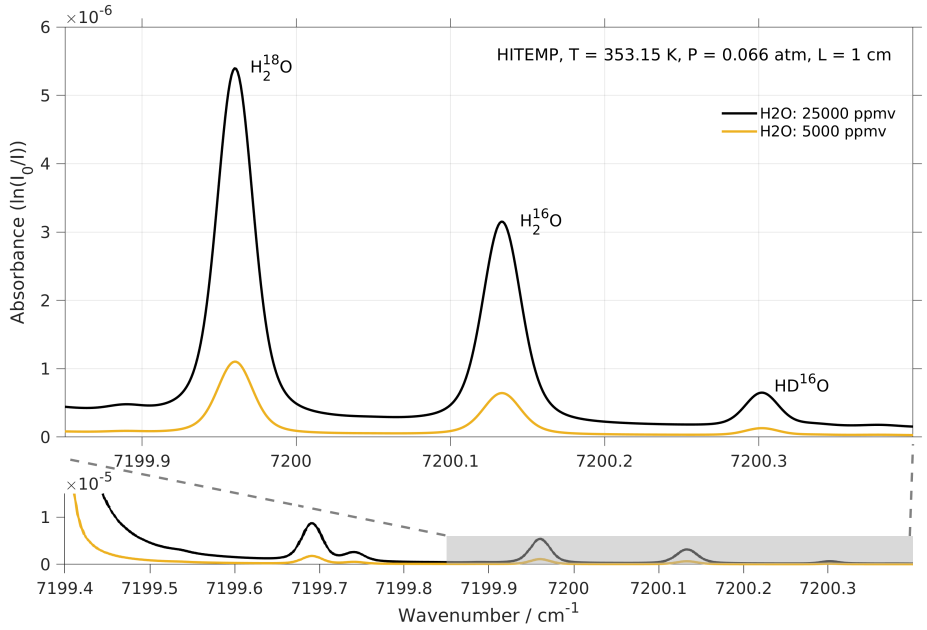

Figure 5. Absorption spectrum of $H_2^{18}O$, $H_2^{16}O$ and $HD^{16}O$ in the frequency range targeted by the laser of Picarro L2130-i and L2140-i. Simulations with two water concentrations, i.e., $25'000$ (black line) and $5'000$ ppmv (orange line), were performed using spectraplot.com with HITRAN/HITEMP database (Goldenstein et al., 2017). Simulation parameters are set according to the cavity conditions of the Picarro analyser: $T = 80$ °C, $P = 50$ Torr and $L = 1$ cm. The upper panel is the zoomed vision of the shaded area in the lower panel.

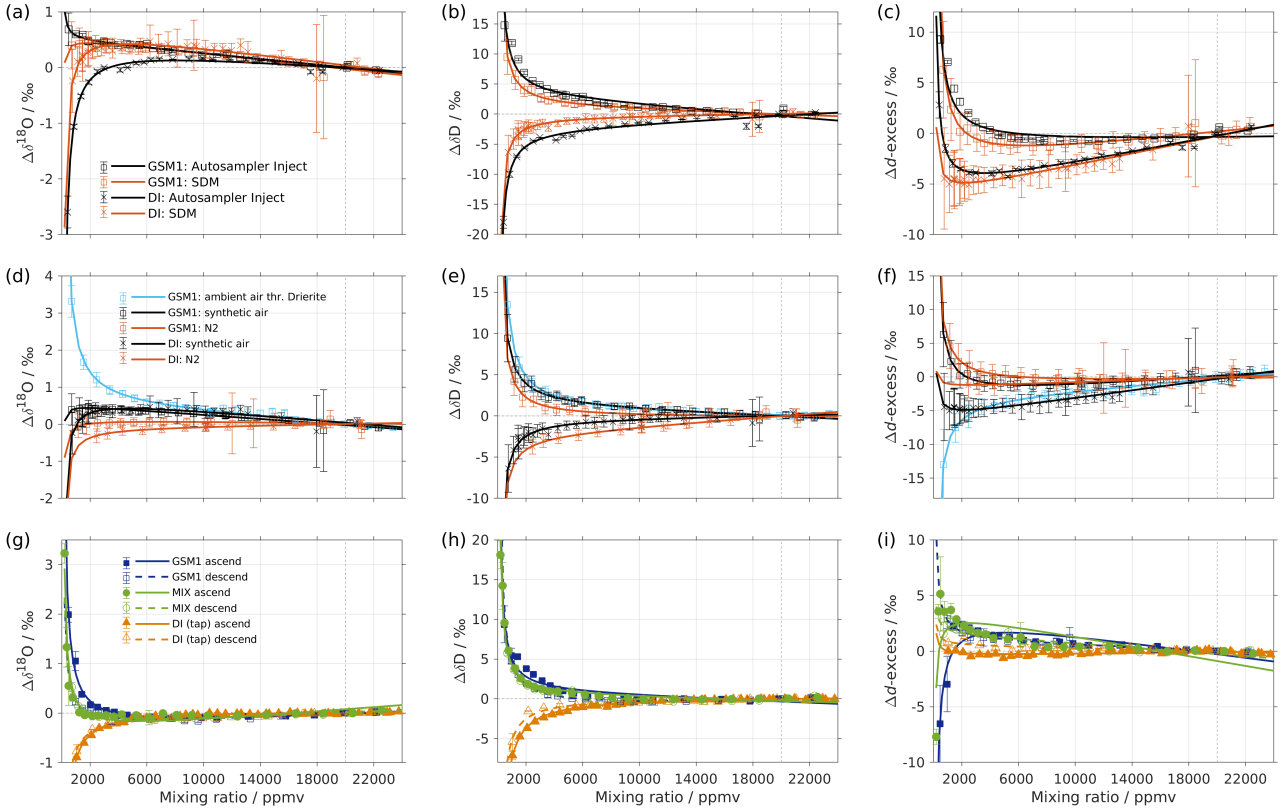

Figure A1. (a-c) Comparison of the isotope composition–mixing ratio dependency of uncalibrated measurements with two different characterisation methods for **(a)** δ^{18}O, **(b)** δD and **(c)** *d*-excess. The measurements are carried out on instrument HIDS2254 (Picarro L2130-i), either with discrete injections using an autosampler (black symbols, experiment 2), or with continuous vapour streaming using the SDM (red symbols, experiment 6), both using synthetic air as the carrier gas. Symbol and error bar represents the mean and standard deviation of the mean for the last three of four injections for the measurement via the autosampler and the mean and standard deviation of the last 2–5 min of a 20–30 min long sequence for the measurement via SDM. Solid line represents the fit using the same function as in Fig. 1. **(d-f)** Same as **(a-c)**, but comparing between different carrier gases. The measurements are carried out on instrument HIDS2254 (Picarro L2130-i) with continuous vapour streaming via SDM (experiment 6–8). Two standard waters (GSM1 and DI) are tested with synthetic air (black symbol) and N_2 (orange symbol). The standard water GSM1 is also tested with ambient air that is dried through Drierite (blue symbol). **(g-i)** Mixing ratio dependency of GSM1 (dark blue symbol), MIX (light blue symbol) and TAP water (orange symbol), with ascending (closed symbol) and descending (open symbol) mixing ratio sequences. Solid curves represent the fits for ascending mixing ratio sequences and dashed curves the fits for descending mixing ratio sequences. All the measurements are uncalibrated and carried out with discrete injections using an autosampler with N_2 being the carrier gas. The measurements for TAP and MIX are carried out on instrument HKDS2038 (Picarro L2140-i) (experiment 9 and 11). The measurements for GSM1 are carried out on instrument HKDS2039 (Picarro L2140-i) and one outlier around 500 ppmv has been excluded (experiment 15).

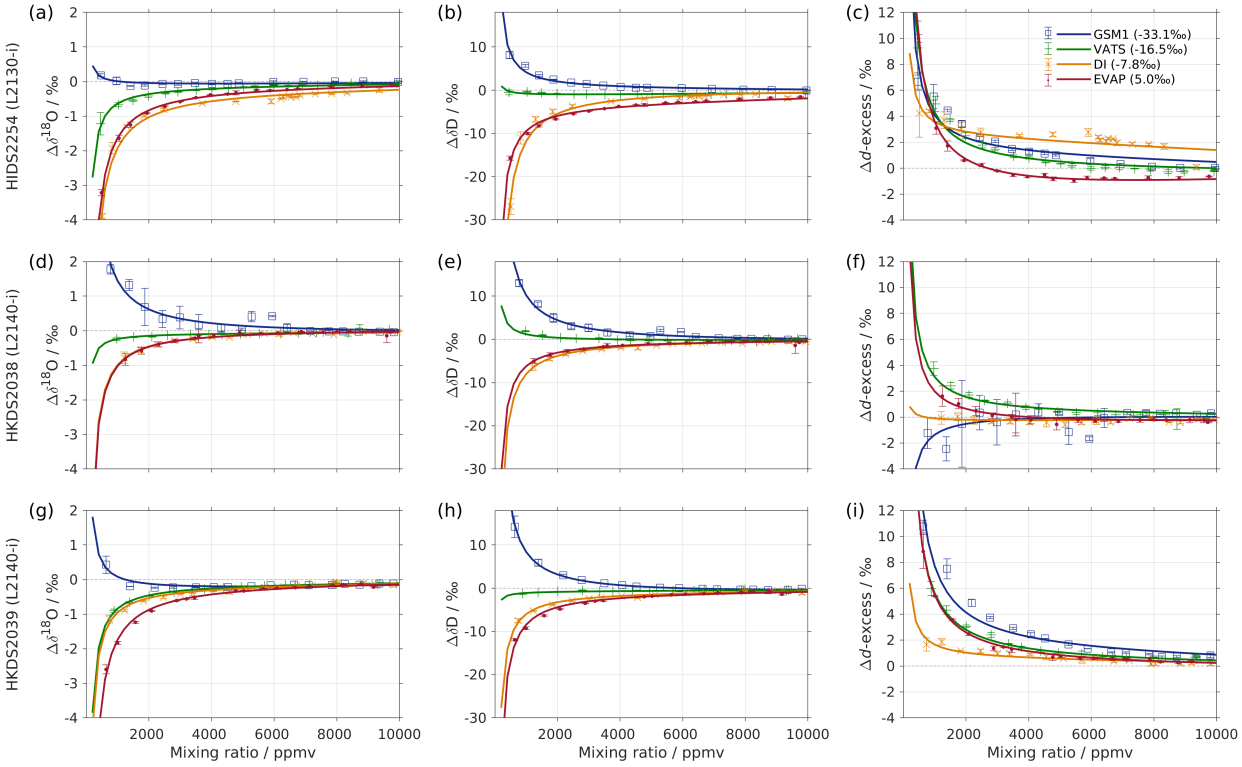

Figure A2. Mixing ratio dependency of uncalibrated measurements for instruments **(a)–(c)** HIDS2254; **(d)–(f)** HKDS2038 and **(g)–(i)** HKDS2039. The measurements are carried out with discrete injections using an autosampler with N_2 as carrier gas (experiment 3, 9 and 14). Only the data below $10'000$ ppmv are shown. Symbols and solid lines indicate measurements and fits respectively as in Fig.1.

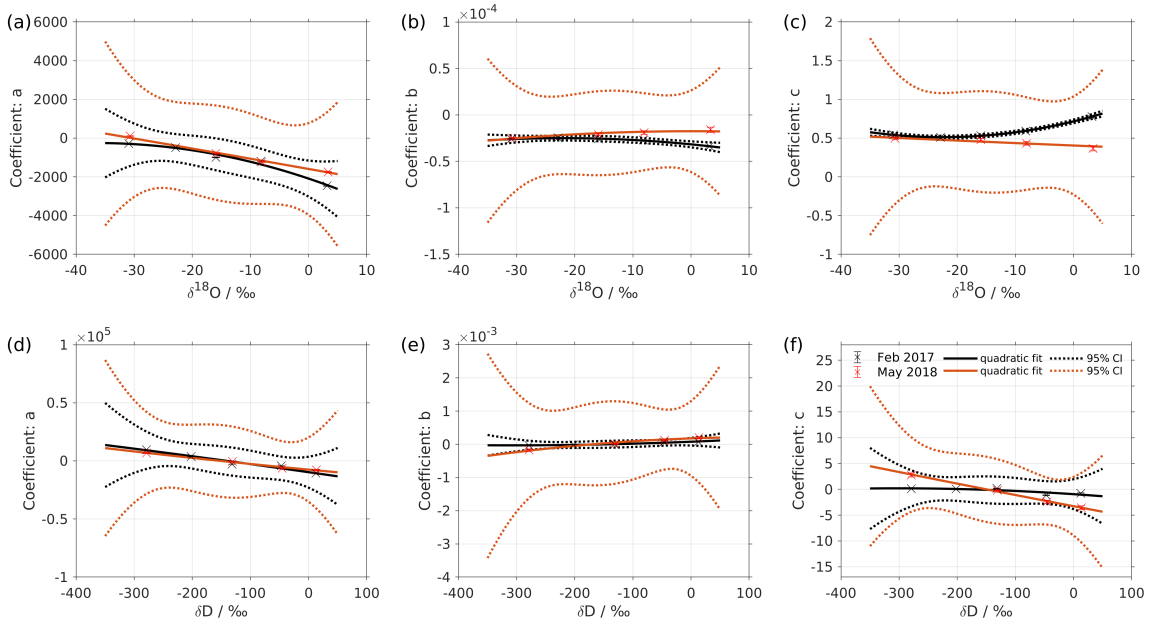

Figure A3. Same as Fig. 2, but a comparison between results in Feb 2017 (black symbols, experiment 1) and May 2018 (red symbols, experiment 2). A larger 95 % confidence interval for the fit of May 2018 (red dotted line) is due to the fewer available data points (only four standards measured).

Table 1. Overview of all 14 characterisation experiments regarding the instrument, the vapour generation method, the type of dry gas supply, the measured standard waters, the mixing ratio steps, the mixing ratio span and the experiment time. For characterisations with injections, typically four injections are carried out at each mixing ratio. For characterisation with continuous vapour streaming via SDM, normally 20–40 min of measurement is carried out at each mixing ratio. The values of the water concentrations are the uncalibrated values measured on the corresponding analyser. Instrument HIDS2254 is model type L2130-i, while instruments HKDS2038 and HKDS2039 are of model type L2140-i.

No.	Instrument	Method	Dry gas	Standard water	Steps	Span [ppmv]	Time
1	HIDS2254	autosampler	synthetic air	GSM1, MIX, VATS, DI, EVAP	47–49	∼500–23000	Feb 2017
2		autosampler	synthetic air	GSM1, VATS, DI, EVAP	27–30	∼1000–23000	May 2018
3		autosampler	N_2	GSM1, VATS, DI, EVAP	25–29	∼500–23000	May 2018
4		SDM	synthetic air	DI	24	∼700–23000	Jul 2016
5		SDM	synthetic air	DI	11	∼1300–20000	Feb 2018
6		SDM	synthetic air	GSM1, DI	23,27	∼700–23000	Jun 2018
7		SDM	N_2	GSM1, DI	13,16	∼1200–23000	Jun 2018
8		SDM	air thr. Drierite	GSM1	27	∼700–23000	Dec 2016
9	HKDS2038	autosampler	N_2	GSM1, MIX, VATS, TAP, EVAP	42–44	∼800–27000	Jan 2017
10		autosampler	N_2	GSM1, VATS, DI	36,29,19	∼600–30000	Feb 2018
11		autosampler	N_2	MIX	19	∼300–23000	Dec 2019
12		manual injection	synthetic air	NEEM, GV, BERM	8	∼2400–24000	Feb 2018
13		manual injection	synthetic air	NEEM, GV, BERM	8	∼2600–22000	Mar 2018
14	HKDS2039	autosampler	N_2	GSM1, MIX, VATS, DI, EVAP	45–47	∼500–27000	Jan 2017
15		autosampler	N_2	GSM1	20	∼500–24000	Jul 2019

Table 2. Isotope compositions of the standard waters used in this study. The values are reported on the VSMOW2-SLAP2 scale. *FARLAB standards* are the laboratory standards in use at FARLAB, University of Bergen and *UI standards* are the laboratory standards in use at the Isotope Laboratory of University of Iceland. All the waters are laboratory working standards except MIX and TAP. MIX is obtained from an even mixing of GSM1 and VATS. TAP is deionised tap water in Bergen, Norway. The isotope compositions of these two waters are calibrated in experiment 9 using the measured working standards. σ for *FARLAB standards* represents the standard deviation of the mean for the six liquid injections, while σ for *UI standards* a long term standard deviation.

	δ^{18}O [‰]	σ [‰]	δD [‰]	σ [‰]	*d*-excess [‰]	σ [‰]
FARLAB standards						
GSM1	-33.07	± 0.02	-262.95	± 0.04	1.63	± 0.17
MIX	-24.78	± 0.02	-193.90	± 0.08	4.30	± 0.20
VATS	-16.47	± 0.02	-127.88	± 0.09	3.89	± 0.18
DI	-7.78	± 0.01	-50.38	± 0.02	11.83	± 0.10
TAP	-7.98	± 0.01	-52.89	± 0.05	10.97	± 0.13
EVAP	5.03	± 0.02	4.75	± 0.11	-35.47	± 0.16
UI standards						
NEEM	-33.52	± 0.05	~~-257.11~~ -257.1	± 0.6	11.05	± 0.72
GV	-8.54	± 0.05	~~-57.72~~ -57.7	± 0.6	10.60	± 0.72
BERM	0.52	± 0.05	~~6.26~~ 6.3	± 0.6	2.10	± 0.72

Table 3. Summary of experiment design, ordered by the aims including the dependency on vapour generating method, the dependency on the tested instrument, the long term stability of the dependency behaviour, the influence from dry gas supply and the influence from the measuring sequence.

Experiments	Factor	Instrument	Parameters	Figure
2, 6	vapour generation	HIDS2254	synthetic air	A1 (a-c)
3, 7	vapour generation	HIDS2254	N_2	not shown
6, 7, 8	dry gas supply	HIDS2254	synth. air, N_2, Drierite, SDM	A1 (d-f)
2, 3	dry gas supply	HIDS2254	synth. air, N_2, autosampler	not shown
9, 11, 15	measuring sequence	HKDS2038, HKDS2039	autosampler, N_2	A1 (g-i)
3, 9, 14	instrument type	HIDS2254, HKDS2038, HKDS2039	autosampler, N_2	A2
1, 2	long term stability (15 months)	HIDS2254	autosampler, synthetic air	A3
4, 5, 6	long term stability (20–25 months)	HIDS2254	SDM, synthetic air	not shown
9, 10	long term stability (11 months)	HKDS2038	autosampler, N_2	not shown
12, 13	long term stability (1 month)	HKDS2038	manual inj., synthetic air	not shown

Table 4. Fitting coefficients for the mixing ratio dependency behaviour of the five standard waters measured on HIDS2254. Coefficients a, b, c are with respect to fitting function $f_\delta(x) = \frac{a_\delta}{x} + b_\delta \cdot x + c_\delta$. The reported uncertainty is one standard deviation. The fitting lines are shown in Fig. 1.

	Standard	a	b	c
δ^{18}O	GSM1	~~-274.95~~ -275 ± ~~16.62~~ 17	-2.60×10^{-5} ± ~~6.237~~6.2×10^{-7}	0.54 ± 0.01
	MIX	~~-488.93~~ -489 ± ~~9.36~~ 10	-2.47×10^{-5} ± ~~4.735~~4.7×10^{-7}	0.51 ± 0.01
	VATS	~~-996.35~~ -996 ± ~~14.46~~ 15	-2.59×10^{-5} ± ~~4.195~~4.2×10^{-7}	0.53 ± 0.01
	DI	~~-1195.79~~ -1200 ± ~~6.53~~ 7	-2.71×10^{-5} ± ~~3.284~~3.3×10^{-7}	0.59 ± 0.01
	EVAP	~~-2465.30~~ -2470 ± ~~20.33~~ 20	-3.39×10^{-5} ± ~~7.958~~8×10^{-7}	0.78 ± 0.01
δD	GSM1	~~9511.99~~ 9510 ± ~~163.45~~ 170	-2.96×10^{-5} ± ~~6.136~~6.2×10^{-6}	0.12 ± 0.10
	MIX	~~3663.09~~ 3660 ± ~~85.40~~ 90	-1.47×10^{-5} ± ~~4.324~~4.4×10^{-6}	0.07 ± 0.07
	VATS	~~-2778.43~~ -2780 ± ~~64.83~~ 70	~~-6.71~~-6.70×10^{-7} ± 1.88×10^{-6}	0.17 ± 0.03
	DI	~~-4219.07~~ -4220 ± ~~73.51~~ 80	6.93×10^{-5} ± ~~3.693~~3.7×10^{-6}	-1.15 ± 0.06
	EVAP	~~-10648.36~~ -10600 ± ~~168.65~~ 200	7.23×10^{-5} ± ~~6.596~~6.6×10^{-6}	-0.79 ± 0.11

Table 5. Fitting coefficients for the isotope composition dependency of the mixing ratio dependency coefficients a, b and c in Table 4. Coefficients m, n and k are with respect to fitting function $f_j(\delta) = m_j(\delta - n_j)^2 + k_j$. The reported uncertainty is one standard deviation. The fitting lines are shown in Fig. 2.

	Coefficient	m	n	k
δ^{18}O	a	-1.38 ± 1.26	~~-36.53~~ -36.5 ± ~~21.48~~ 21.5	~~-252.68~~ -253 ± ~~582.52~~ 583
	b	-1.38×10^{-8} ± ~~4.394~~4.4×10^{-9}	-22 ± ~~3.12~~ 4	-2.50×10^{-5} ± ~~7.168~~7.2×10^{-7}
	c	4.05×10^{-4} ± ~~3.183~~3.2×10^{-5}	~~-22.43~~ -22.4 ± ~~0.80~~ 0.8	0.51 ± 0.01
δD	a	-0.01 ± 0.25	~~-3224.26~~ -3220 ± ~~69244.35~~ 69300	1.04×10^{5} ± 2.35×10^{6}
	b	1.13×10^{-9} ± 2.12×10^{-9}	-310 ± ~~341.73~~ 342	-3.07×10^{-5} ± 5.73×10^{-5}
	c	-1.23×10^{-5} ± 5.33×10^{-5}	~~-302.62~~ -303 ± ~~758.25~~ 759	0.19 ± 1.32